Environmental Science & Technology

pubs.acs.org/est

Critical Review

Spectrophotometric Measurement of Carbonate Ion in Seawater over a Decade: Dealing with Inconsistencies

Elisa F. Guallart,*,□ Noelia M. Fajar, Maribel I. García-Ibáñez, Mónica Castaño-Carrera, Rocío Santiago-Doménech, Abed El Rahman Hassoun, Fiz F. Pérez, Regina A. Easley, and Marta Álvarez□

Cite This: *Environ. Sci. Technol.* 2022, 56, 7381−7395

Read Online

ACCESS | Metrics & More | Article Recommendations | Supporting Information

ABSTRACT: The spectrophotometric methodology for carbonate ion determination in seawater was first published in 2008 and has been continuously evolving in terms of reagents and formulations. Although being fast, relatively simple, affordable, and potentially easy to implement in different platforms and facilities for discrete and autonomous observations, its use is not widespread in the ocean acidification community. This study uses a merged overdetermined CO_2 system data set (carbonate ion, pH, and alkalinity) obtained from 2009 to 2020 to assess the differences among the five current approaches of the methodology through an internal consistency analysis and discussing the sources of uncertainty. Overall, the results show that none of the approaches meet the climate goal (± 1 % standard uncertainty) for ocean acidification studies for the whole carbonate ion content range in this study but usually fulfill the weather goal (± 10 % standard uncertainty). The inconsistencies observed among approaches compromise the consistency of data sets among regions and through time, highlighting the need for a validated standard operating procedure for spectrophotometric carbonate ion measurements as already available for the other measurable CO_2 variables.

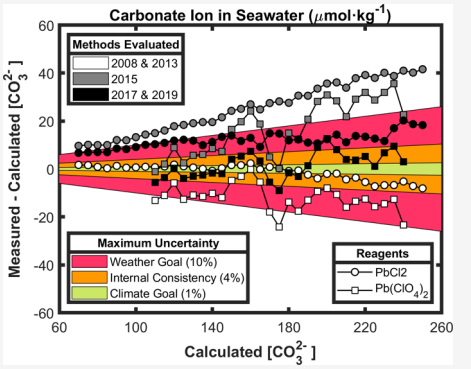

KEYWORDS: *ocean acidification, saturation states, bio-geochemistry, oceanic carbon cycle, time-series, CO_2 system monitoring, CO_2 system variables, climate goal*

1. INTRODUCTION

About a third of the global anthropogenic carbon dioxide (CO_2) emissions have been absorbed by the global ocean since the preindustrial era.[1] By acting as a sink of atmospheric CO_2, the ocean contributes to decreasing the rate at which climate change occurs. Nevertheless, such an effect is counteracted by the resulting increase in seawater acidity (ocean acidification, OA), which determines a decrease in the amount of carbonate ion content in seawater ($[CO_3^{2-}]$) and therefore of buffering capacity of the ocean.[2−6]

The overall concern for the sustainability of marine life and resources has mobilized the international community to coordinate efforts to track long-term trends in OA by observing seawater CO_2 variables in coastal[7] and open ocean[8,9] time-series. The measurable seawater CO_2 variables (dissolved inorganic carbon (DIC), total alkalinity (TA), partial pressure of CO_2 (pCO_2), and pH) are included by the Global Ocean Observing System (GOOS) as Essential Ocean Variables (EOVs) to constrain the CO_2 system changes and drivers in seawater. Identified and predicted bio-geochemical[10,11] and ecological[12−14] OA implications are related to changes in the saturation state (Ω) of seawater for calcium carbonate ($CaCO_3$) minerals,[2,11,15] which control the precipitation and dissolution of its aragonite and calcite forms depending on the available in situ $[CO_3^{2-}]$.[16] As the oceans acidify, the location and extent of the regions where $CaCO_3$ dissolution occurs are expected to increase,[11,15] particularly in regions with low buffer capacity (Appendix A in Supporting Information).

The increasing amount of CO_2 data produced demands quality-controlled measurements to ensure their intercomparison. Regarding the four measurable seawater CO_2 system variables, standard procedures of analysis, data quality control, and reporting are widely established.[17,18] Additionally, to improve the spatiotemporal resolution of the observation of the seawater CO_2 system, intensive effort has been made to implement standardized procedures for in situ autonomous measurements performed by autonomous vehicles.[19,20] Accordingly, relatively simple, fast, and precise automated methods for discrete measurements are encouraged to be implemented.[21] In this regard, most studies would benefit from moving $[CO_3^{2-}]$

Received: September 8, 2021
Revised: April 12, 2022
Accepted: April 13, 2022
Published: June 7, 2022

from its category of a derived variable to become the fifth measurable seawater CO_2 system variable, thus allowing efficient ways of approaching questions relative to $CaCO_3$ cycling from $[CO_3^{2-}]$ direct determinations.[22,23] To this end, Byrne and Yao[24] first proposed a spectrophotometric method to determine $[CO_3^{2-}]$ in seawater. This method is proposed to be ready for implementation in sustained observations and internal consistency studies.[25,26] However, its implementation still needs to be validated by independent research groups.

The methodology for the quantification of spectrophotometric $[CO_3^{2-}]$ ($[CO_3^{2-}]_{spec}$) relies on the speciation of lead (Pb(II)) in seawater over a particular pH range (7.7−8.2) at which the complexation of Pb(II) and CO_3^{2-} predominantly occurs.[27] The main details on the theory behind the methodology and its evolution are summarized below. A detailed explanation of the motivation for such methodological changes can be found in the Supporting Information (Appendix B) and the related literature.[24,25,27−33]

$[CO_3^{2-}]_{spec}$ is determined by quantifying the ultraviolet light absorbed by lead carbonate, lead chloride/sulfate species, and free Pb^{2+} in Pb(II)-enriched seawater through the following expression:

$$-\log[CO_3^{2-}]_{spec} = \log\left[\frac{{}_{CO_3}\beta_1}{e_2}\right] + \log\left[\frac{R - e_1}{1 - R\cdot\frac{e_3}{e_2}}\right] \quad (1)$$

where ${}_{CO_3}\beta_1$ is the associated equilibrium constant for the complexation of Pb^{2+} and $[CO_3^{2-}]$, and R is the absorbance (A) ratio of Pb(II) species at 234 nanometers (nm) and 250 nm, corrected for the background absorbance at 350 nm:

$$R = \frac{{}_{250}A - {}_{350}A}{{}_{234}A - {}_{350}A} \quad (2)$$

The molar absorptivity ratios e_1, e_2, and e_3/e_2 are defined as

$$e_1 = \frac{{}_{250}\varepsilon_{PbCO_3}}{{}_{234}\varepsilon_{PbCO_3}}, \quad e_2 = \frac{{}_{250}\varepsilon_{Pb}}{{}_{234}\varepsilon_{PbCO_3}}, \quad e_3/e_2 = \frac{{}_{234}\varepsilon_{Pb}}{{}_{250}\varepsilon_{Pb}} \quad (3)$$

Equation 1 has the same form as the one used to determine spectrophotometric pH on the total pH scale[34] and allows quantifying $[CO_3^{2-}]_{spec}$ with a minimum number of parameters via a procedure that closely follows that of spectrophotometric pH. However, unlike other measurable CO_2 system variables, no recommended standard operating procedure (SOP) has been established for measuring $[CO_3^{2-}]_{spec}$, nor are certified reference materials (CRMs) available for this variable.[17]

The first approach for measuring $[CO_3^{2-}]_{spec}$ was described by Byrne and Yao[24] in 2008 (BY08). During the following decade, the method was refined by Easley et al.[28] (EAS13), Patsavas et al.[29] (PAT15), Sharp et al.[30] (SHA17), and Sharp and Byrne[25] (SHA19) in terms of the procedure for obtaining accurate R data and, more importantly, the calibration or fitting of the parameters $\log\{{}_{CO_3}\beta_1/e_2\}$, e_1, and e_3/e_2 (eq 1) needed to relate a particular R value (eq 2) with $[CO_3^{2-}]$ (Appendix B).

The former works of BY08 and EAS13 used Pb(II) chloride ($PbCl_2$) as the reagent to obtain the R measurements. PAT15 proposed a change to Pb(II) perchlorate ($Pb(ClO_4)_2$) and recommended an additional procedure to correct R data for sample perturbation due to reagent addition, as

$$\log(R - R^0) = -17.6664\cdot R^2 + 19.8995\cdot R - 7.7324 \quad (4)$$

where R^0 corresponds to the unperturbed R value. After SHA17, R measurements were no longer corrected with eq 4 but readjusted to include an offset correction for wavelength calibration inaccuracies of the spectrophotometer (R^0), as

$$R^0 = R + 0.0265\cdot\Delta\lambda_{241.1} \quad (5)$$

where $\Delta\lambda_{241.1}$ is the spectrophotometer-specific wavelength offset, defined as the difference between the wavelength location of a holmium oxide standard absorbance peak at 241.10 nm specified by the manufacturer minus the wavelength at which the spectrophotometer reports the peak. The sign of eq 5 is reversed with regard to SHA17, where there was an error in the reported equation (J. D. Sharp, personal communication). R^0 refers to the true R value for PAT15 and SHA17. Finally, SHA19 followed SHA17 to obtain R^0 but reported the most recent characterization of the terms in eq 1, extending their suitability to a larger range of temperatures and salinities. Before SHA19, the method was solely characterized for use at 25 °C.

All five approaches (Table S1) for $[CO_3^{2-}]_{spec}$ determination are valid for given oceanographic conditions, and none clearly invalidates the others.[24,25,28−30] In this study, the evolution of the $[CO_3^{2-}]_{spec}$ methodology is evaluated through an internal consistency analysis of a field-based data set obtained during 2009−2020 and expanding over a broad range of oceanographic conditions. A detailed assessment of the different sources of uncertainty in $[CO_3^{2-}]_{spec}$ is discussed. Finally, difficulties found concerning the implementation of the methodology are highlighted.

2. MATERIALS AND METHODS

2.1. Cruise Data Compilation. Hydrographic and chemical data from nine open ocean cruises in the North Atlantic Ocean and the Mediterranean Sea, and one coastal time-series in the North-East Atlantic Ocean, performed during 2009−2020 (Figure 1 and Table 1), were compiled for assessing the evolution of the $[CO_3^{2-}]_{spec}$ methodology. All data sets include paired measurements of $[CO_3^{2-}]_{spec}$, pH, and TA, and some also include DIC measurements. All seawater CO_2 system variables were measured following the corresponding SOPs[17] except

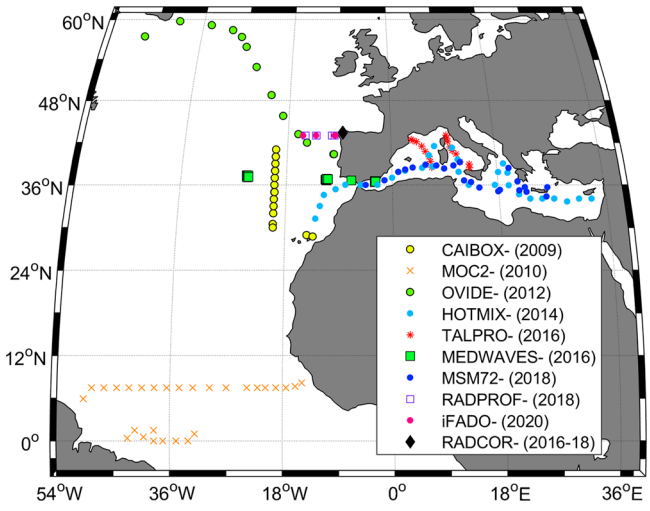

Figure 1. Location of the hydrographic stations of nine open ocean cruises and one coastal time-series site where spectrophotometric carbonate ion content ($[CO_3^{2-}]_{spec}$), pH, TA, and DIC were measured, during 2009−2020. See Table 1 for further details.

https://doi.org/10.1021/acs.est.1c06083
Environ. Sci. Technol. 2022, 56, 7381−7395

Table 1. Cruise Summary Information Containing the Cruise Alias and Assigned EXPOCODE, Research Vessel and Year of Performance, and Ocean Region Studied[a]

Cruise Alias, EXPOCODE	Research vessel, year	Region	Pb(II) reagent(N)	Precision mean ± STD (μmol·kg^{-1}) (%)	spectroph. $[CO_3^{2-}]_{spec}$/pH	Salinity range	pH range	TA range (μmol·kg^{-1})	$[CO_3^{2-}]_{calc}$range (μmol·kg^{-1})	TA/DIC range
CAIBOX, 29AH20090725	R/V *Sarmiento de Gamboa*, 2009	North East Atlantic	$PbCl_2$ (272)	225.0 ± 2.9 (1.3 %)	PE850/SHI2401	34.89−37.08	7.65−8.03	2305−2428	101−227	1.05−1.15
MOC2, 29HE20100405	R/V *Hesperides*, 2010	Equatorial Atlantic	$PbCl_2$ (625)	249.0 ± 3.4 (1.4 %)	SHI2401	34.50−36.72	7.47−8.13	2294−2408	68−252	1.02−1.18
HOTMIX, 29AH20140426	R/V *Meteor*, 2011	Mediterranean Sea	$PbCl_2$ (328)	214.0 ± 2.6 (1.2 %)	SHI2600	34.89−39.24	7.72−8.02	2330−2634	118−250	1.07−1.15
OVIDE, 29AH20120623	R/V *Sarmiento de Gamboa,* 2012	Subpolar North Atlantic	$PbCl_2$ (196)	129.0 ± 1.6 (1.2 %)	PE850	34.46−36.23	7.69−7.99	2292−2398	109−201	1.06−1.13
TALPRO, 29AJ20160818	R/V *Angeles Alvariño,* 2016	Western Mediterranean Sea	$Pb(ClO_4)_2$ (115)	211.0 ± 7.0 (4 %)	BK800	37.30−38.82	7.88−8.02	2476−2620	187−242	1.11−1.15
MEDWAVES, N/A	R/V *Sarmiento de Gamboa*, 2016	North Eastern Atlantic and Alboran Sea	$Pb(ClO_4)_2$ (148)	131.0 ± 1.0 (0.6 %)	PE850	34.93−38.54	7.70−8.01	2310−2590	111−212	1.06−1.14
MSM72, 06M2201S0302	R/V *Maria S. Merian*, 2018	Mediterranean Sea	$Pb(ClO_4)_2$ (294)	238.0 ± 1.0 (0.4 %)	SHI2600	36.45−39.29	7.86−7.99	2397−2639	179−239	1.10−1.14
RADPROF, N/A	R/V *Ramon Margalef*, 2018	Iberian Basin North East Atlantic	$PbCl_2$ (50)	l31.0 ± 0.8 (0.6 %)	SHI2600	34.90−36.02	7.72−7.97	2316−2383	116−193	1.07−1.13
			$Pb(ClO_4)_2$ (46)	l26.0 ± 2.5 (2 %)						
RADCOR, N/A	R/V-*Lura,* 2016 to 2018	North West Galician Coast	$PbCl_2$ (128)		SHI2600	33.72−35.74	7.78−8.02	2249−2361	131−200	1.08−1.14
			$Pb(ClO_4)_2$ (74)							
iFADO, N/A	R/V *Sarmiento de Gamboa*, 2020	Iberian Basin North East Atlantic	$PbCl_2$ (29)	126.0 ± 2.2 (1.7 %)	SHI2600	34.89−36.13	7.72−7.96	2315−2390	115−188	1.07−1.13
			$Pb(ClO_4)_2$ (32)	122.0 ± 1.0 (1 %)						
iFADO2, N/A	R/V *Sarmiento de Gamboa*, 2020	Iberian Basin North East Atlantic	$PbCl_2$ (33)	127.0 ± 4.9 (3.9 %)	PE850/SHI2600	34.89−36.13	7.72−7.96	2315−2389	115−188	1.07−1.13
			$Pb(ClO_4)_2$ (34)	122.0 ± 2.0 (1.7 %)						

[a]Information relative to $[CO_3^{2-}]_{spec}$: Pb(II) reagent and number of measurements (N); precision in μmol·kg^{-1} and % (mean $[CO_3^{2-}]_{spec}$ ± standard deviation, STD, of the measured replicates is also shown). The spectrophotometer (spectroph.) used for obtaining $[CO_3^{2-}]_{spec}$ and pH is indicated. The ranges of main variables are shown: salinity, pH (total scale at 25 °C), total alkalinity (TA), calculated carbonate ion content ($[CO_3^{2-}]_{calc}$ at 25 °C from pH-TA pair), and TA/DIC ratio (DIC calculated from pH-TA). The reagent $PbCl_2$ was 1.1 mmol·L^{-1}, and 250 μL (CAIBOX, MOC2, and OVIDE) or 225 μL (rest of cruises) were added. The $Pb(ClO_4)_2$ reagent was 22 mmol·L^{-1}, and 20 μL were added.

https://doi.org/10.1021/acs.est.1c06083
Environ. Sci. Technol. 2022, 56, 7381−7395

$[CO_3^{2-}]_{spec}$ that lacks an SOP. As ancillary data, this study uses hydrographic CTD data and inorganic nutrients (silicate and phosphate). The compiled data set is publicly available in Alvarez et al.[35]

A solution of unpurified *m*-cresol purple (2 mmol·L^{-1}) was used for spectrophotometric pH measurements.[34] All pH data are reported on the total hydrogen ion scale at 25 °C and atmospheric pressure (hereafter pH). The overall pH precision for all cruises is ± 0.003 pH units based on sample replicates, while the assigned total uncertainty is considered as ± 0.01 pH units (Appendix C).[36−38] TA samples were measured following a double end-point potentiometric titration,[39−41] and DIC samples were analyzed through coulometric determination.[42] TA and DIC accuracies were verified with CRMs.[43] The TA and DIC precision is ± 2 μmol·kg^{-1} based on sample replicates, and the total uncertainty is ± 3 μmol·kg^{-1} for both TA and DIC.[36] pH and TA measurements were performed onboard except for the RADCOR time-series, where samples were analyzed at the Instituto Español de Oceanografía (IEO) laboratory the same day and within 2 days after sampling, respectively. DIC measurements were mostly performed postcruise at the IEO laboratory on stored samples poisoned with a saturated solution of mercuric chloride ($HgCl_2$), except for the TALPRO and MSM72 cruises during which DIC measurements were performed onboard. Further cruise details are in Table 1.

The overall $[CO_3^{2-}]_{spec}$ measurement procedure has remained the same during the study period. Seawater samples were collected from the Niskin bottles directly into 10 cm quartz cuvettes (~30 mL volume) that were immediately capped with Teflon caps and heated to 25 °C. All spectrophotometric analyses were performed manually. For each cuvette, a baseline (seawater only) measurement was first performed and followed by the addition of the Pb(II) reagent. Absorbance measurements were recorded in triplicate at three wavelengths (234 nm, 250 nm, and 350 nm) to get an averaged absorbance ratio (R; eq 2) for each sample. The temperature of each sample was recorded immediately with a temperature probe (± 0.03 °C) after the absorbance measurements. The Pb(II) reagent, stock concentration, volume addition, and spectrophotometer used for each cruise are detailed in Table 1. Spectrophotometer specifications are detailed in Table S3. Except for CAIBOX and iFADO, pH and $[CO_3^{2-}]_{spec}$ samples were always analyzed with the same spectrophotometer (Table 1). For iFADO, two different spectrophotometers were used onboard for comparison. The precision of the $[CO_3^{2-}]_{spec}$ measurements was evaluated through replicate analysis during each cruise and ranged between ± 1 μmol·kg^{-1} and ± 6.9 μmol·kg^{-1} (± 0.4 % and ± 4 %) (Table 1).

One of the main analytical changes in the methodology reported during the study period implies a change in the Pb(II) reagent from $PbCl_2$ (BY08 and EAS13) to $Pb(ClO_4)_2$ (PAT15, SHA17, and SHA19) (Appendix B). In this study, 1666 samples were measured with $PbCl_2$ in cruises performed during 2009−2012 (CAIBOX, MOC2, HOTMIX, and OVIDE), and 743 with $Pb(ClO_4)_2$, during 2016−2020 (TALPRO, MEDWAVES, and MSM72). Double measurements with $PbCl_2$ and $Pb(ClO_4)_2$ were performed in RADCOR, RADPROF, and iFADO during 2018−2020 (Table 1).

The second major change in the methodology was proposed by SHA17, who recommended readjusting the measured R into an offset-corrected R^0 (eq 5 and Appendix B). In this study, the proposed correction was implemented for the cruises where the SHI2600 spectrophotometer was used (Table 1). The equipment was examined for potential wavelength accuracy offsets using a holmium oxide standard (type 667-UV5, provided by Hellma) to assess the $\Delta\lambda_{241.1}$ term (eq 5). Lacking a detailed wavelength accuracy test procedure in SHA17, all the measurements were performed reproducing the calibration conditions described in the holmium certification. After 15 determinations, which yielded values between 0.1 nm and 0.3 nm, $\Delta\lambda_{241.1}$ was assigned an average value of 0.2 nm, which equals the uncertainty of the certified peak. This offset was applied to R data from HOTMIX, MSM72, RADPROF, iFADO, and RADCOR (Table 1). The PE850 spectrophotometer was also examined during the iFADO cruise, with three determinations, yielding $\Delta\lambda_{241.1}$ equal to zero. For the remaining cruises, we were unable to examine the equipment, or these had been recalibrated after the cruise; therefore, no wavelength offset correction was applied to CAIBOX, MOC2, OVIDE, TALPRO, and MEDWAVES. Small deviations from the reference temperature (25 °C) were accounted for using SHA19 formulations since the temperature was measured for each sample (mean difference in temperature measurement with regard to 25 °C ranged between 0.02 °C and 0.70 °C among data sets).

R values obtained with $PbCl_2$ and $Pb(ClO_4)_2$ were indistinctly used with the different formulations in Tables S1 and S2 and $[CO_3^{2-}]_{spec}$ were calculated using all possible combinations between formulations and reagents, under the following assumption: neither the molecular Pb(II) complex added nor its final concentration in the cuvette should affect the absorbance measurements since the method relies on the characterization of the Pb(II) absorbance signal in seawater.[27] This would be supported by the fact that PAT15 assessed the formulations by BY08 that were obtained with $PbCl_2$ with data measured with $Pb(ClO_4)_2$ and proposed using the same formulation for e_3/e_2 as BY08 (Table S2). Hence, five different $[CO_3^{2-}]_{spec}$ values were obtained for each measured R value. The BY08, EAS13, PAT15, and SHA17 formulations in Table S2 are referred to 25 °C and atmospheric pressure, being a function of R and salinity. Only the formulation by SHA19 is also temperature-dependent. Hereafter, the particular $[CO_3^{2-}]_{spec}$ is noted as $[CO_3^{2-}]_{specX}$, where X is the approach abbreviation (BY08, EAS13, PAT15, SHA17, and SHA19).

Fajar et al.[44] reported $[CO_3^{2-}]_{spec}$ data from the CAIBOX, MOC2, HOTMIX, and OVIDE cruises, comparing BY08 and EAS13 formulations. This study adds new $[CO_3^{2-}]_{spec}$ data from six cruises in the Mediterranean Sea (TALPRO, MEDWAVES, and MSM72) and the northeast Atlantic Ocean (MEDWAVES, RADPROF, RADCOR, and iFADO). The compiled data cover a wide range of oceanographic conditions in terms of salinity (33.7−39.3), pH (7.47 pH units −8.13 pH units), TA (2249 μmol·kg^{-1} − 2639 μmol·kg^{-1}), TA/DIC ratio (1.02−1.18), and the expected $[CO_3^{2-}]$ (68 μmol·kg^{-1} − 252 μmol·kg^{-1}) from coastal to open ocean. These ranges are mostly representative of typical open ocean surface conditions over the global ocean (Appendix A; Figure S1).

2.2. Definition and Uncertainty in $\Delta[CO_3^{2-}]$. The goodness of the five approaches for quantifying $[CO_3^{2-}]_{spec}$ was evaluated in terms of the internal consistency between measured and calculated $[CO_3^{2-}]$ following the works describing the methodology.[24,25,28−30] The internal consistency analysis assesses how well predicted values of $[CO_3^{2-}]$ compare to the expected or reference $[CO_3^{2-}]$ values. To this end, $[CO_3^{2-}]$ residuals were obtained as the difference between measured $[CO_3^{2-}]_{spec}$ and $[CO_3^{2-}]$ calculated from thermodynamic equations with paired CO_2 variables ($[CO_3^{2-}]_{calc}$)

https://doi.org/10.1021/acs.est.1c06083
Environ. Sci. Technol. 2022, 56, 7381−7395

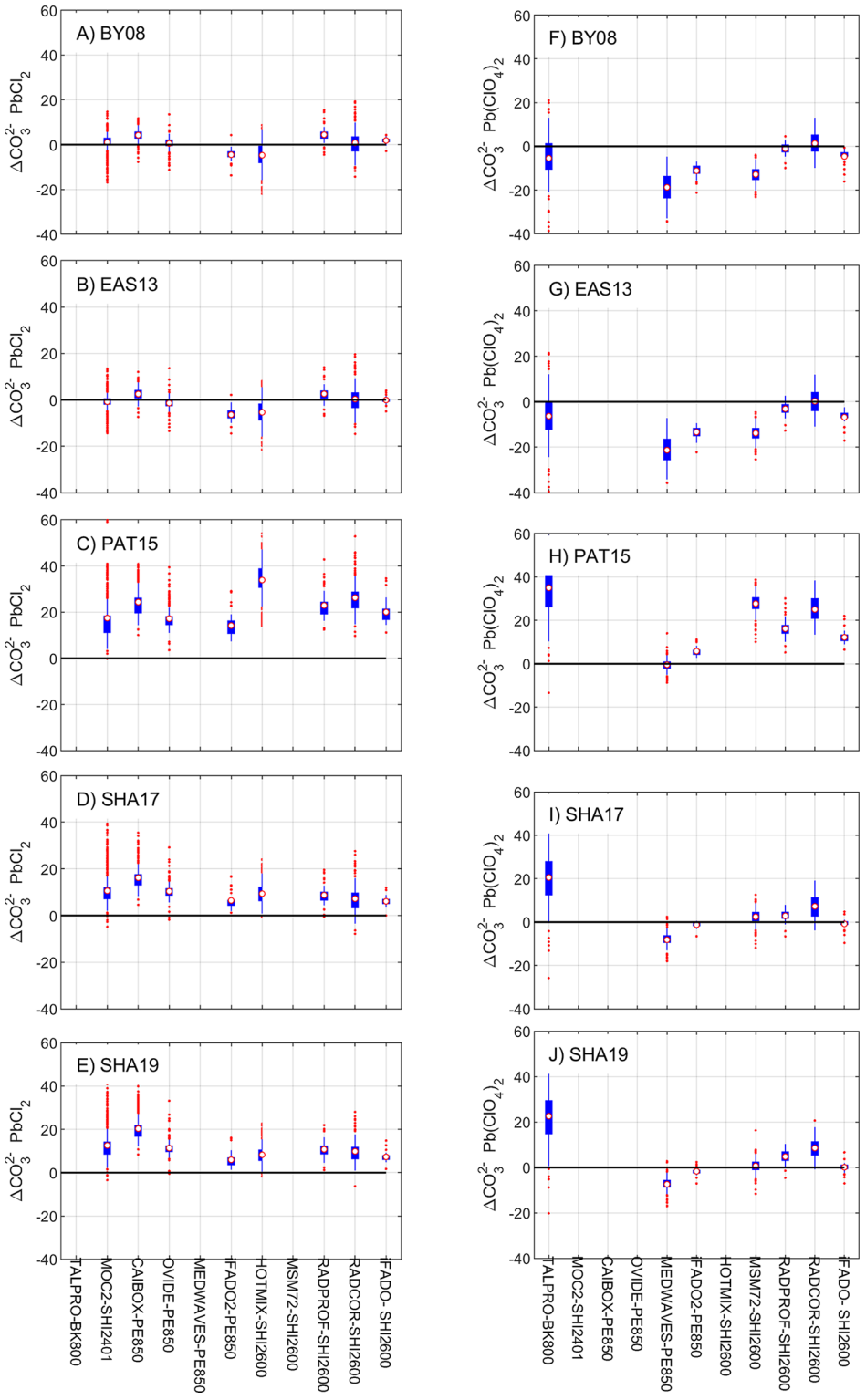

Figure 2. Whisker plots showing spectrophotometric minus calculated carbonate ion content ($\Delta[CO_3^{2-}] = [CO_3^{2-}]_{spec} - [CO_3^{2-}]_{calc}$; in $\mu mol \cdot kg^{-1}$) for cruises in Figure 1 and Table 1. The central dot denotes the mean $\Delta[CO_3^{2-}]$, and the lower and upper limits of the blue box are the first and third quartiles, respectively. Whiskers cover 95% of data variance. Red dots are outliers located beyond one-time the interquartile range. $[CO_3^{2-}]_{spec}$ is obtained with five different formulations (Table S2): (A and F) BY08, (B and G) EAS13, (C and H) PAT15, (D and I) SHA17, and (E and J) SHA19. Left and right panels refer to $[CO_3^{2-}]_{spec}$ data measured with $PbCl_2$ and $Pb(ClO_4)_2$, respectively. The cruise alias and the spectrophotometer model used (Table 1) are indicated as *x*-axis labels. $[CO_3^{2-}]_{calc}$ is calculated with pH-TA. Calculations are reported at 25 °C and atmospheric pressure except for SHA19 that are reported at the exact temperature of analysis. The SHA17 and SHA19 approaches include a wavelength correction ($\Delta\lambda_{241.1} = 0.2$ nm, Table S1) for cruises where the SHI2600 was used (HOTMIX, MSM72, RADPROF, RADCOR, and iFADO; Table 1) and is null for the remaining cruises.

https://doi.org/10.1021/acs.est.1c06083
Environ. Sci. Technol. 2022, 56, 7381−7395

($\Delta[CO_3^{2-}] = [CO_3^{2-}]_{spec} - [CO_3^{2-}]_{calc}$; in $\mu mol \cdot kg^{-1}$). Each of the five $[CO_3^{2-}]_{spec}$ determinations was considered a predicted value, dependent on different sets of calibration functions (Table S2), to be compared to the expected $[CO_3^{2-}]_{calc}$. $[CO_3^{2-}]_{calc}$ was considered the reference value because it is based on paired CO_2 input variables that have solid SOPs, CRMs exist for some of them, and the methodology for measuring $[CO_3^{2-}]_{spec}$ is itself defined according to $[CO_3^{2-}]_{calc}$ (Appendixes B and D).[24,25,28−30] As for $[CO_3^{2-}]_{spec}$, corresponding $\Delta[CO_3^{2-}]$ will be noted as $\Delta[CO_3^{2-}]_X$, where X is the approach abbreviation (BY08, EAS13, PAT15, SHA17, and SHA19).

$[CO_3^{2-}]_{calc}$ was estimated using the MATLAB CO2SYS software,[45] at 25 °C and atmospheric pressure, using both measured pH-TA and TA-DIC pairs, along with total phosphate and silicate. The CO_2 equilibrium constants of Mehrbach et al.[46] reformulated on the total hydrogen scale by Lueker et al.[47] the bisulfate equilibrium constant of Dickson,[48] and the boron to chlorinity ratio of Lee et al.[49] were used for the calculations. Absolute differences between $[CO_3^{2-}]_{calc}$ derived from TA-pH and TA-DIC were not significant (Appendix D). Since paired measurements of pH-TA are more abundant than TA-DIC pairs ($N = 2367$ and $N = 628$, respectively), $[CO_3^{2-}]_{calc}$ results shown refer to $[CO_3^{2-}]_{calc}$ from pH and TA.

Studying the internal consistency of $\Delta[CO_3^{2-}]$ implies studying how well each of the five predicted values of $[CO_3^{2-}]_{spec}$, dependent on different sets of coefficients (Table S2), compare with the expected $[CO_3^{2-}]_{calc}$ within given limits of uncertainty. A limit of uncertainty of ± 4 % of the expected $[CO_3^{2-}]_{calc}$ was obtained by propagating the standard uncertainties of $[CO_3^{2-}]_{spec}$ and $[CO_3^{2-}]_{calc}$. For $[CO_3^{2-}]_{spec}$, the value of ± 2 % standard uncertainty, assigned among approaches (Table S1 and Appendix C), was considered. The total standard uncertainty of $[CO_3^{2-}]_{calc}$ was calculated using the software package *errors* from Orr et al.[37] (Appendix D). For the calculations, the following uncorrelated uncertainties were assigned to the input CO_2 system variables: ± 0.01 pH units for pH, ± 3 $\mu mol \cdot kg^{-1}$ for TA (section 2.1), and the uncertainty for the equilibrium constants was taken from Table 1 in Orr et al.[37] Ancillary variables (temperature, salinity, and pressure) and inorganic nutrients were assumed to have negligible standard uncertainty, as in SHA19. The resulting total uncertainty is proportional to $[CO_3^{2-}]_{calc}$ and ranges between 2.5 $\mu mol \cdot kg^{-1}$ and 8 $\mu mol \cdot kg^{-1}$ (± 3.2 % − ± 3.7 %) for the studied $[CO_3^{2-}]_{calc}$ range (68 $\mu mol \cdot kg^{-1}$ to 252 $\mu mol \cdot kg^{-1}$) (Appendix D; Figure S4). The resulting propagated uncertainty limit to consider $\Delta[CO_3^{2-}]$ internally consistent within the $[CO_3^{2-}]_{calc}$ range in this study ranged from ± 3.8 % to ± 4.2 % and was averaged to ± 4 %.

Internally consistent $\Delta[CO_3^{2-}]$ values will distribute randomly around zero until the ± 4 % limit. Larger $\Delta[CO_3^{2-}]$ values might be due to particularities of each approach, either relative to the respective calibration functions fitting conditions or to the differing methodological recommendations for obtaining *R* values (Table S1). This limit also allows assessing whether there is internal consistency across the five $[CO_3^{2-}]_{spec}$ determinations. Note that the choice of the pH-TA pair implies a more conservative interpretation of the $\Delta[CO_3^{2-}]$ with regard to the TA-DIC pair because of the larger uncertainty in $[CO_3^{2-}]_{calc}$ (Appendix D) and is based on assuming quite large uncertainties in the input variables. In addition, $\Delta[CO_3^{2-}]$ are also evaluated according to the standard uncertainty limits for weather and climate-quality objectives for OA studies recommended by the Global Ocean Acidification Observing Network (GOA-ON)[50] of ± 10 % and ± 1 %, respectively.

3. RESULTS

3.1. Overview of $\Delta[CO_3^{2-}]$ Results. Figure 2 shows an overview of the $\Delta[CO_3^{2-}]$ results by approach, reagent, cruise, and spectrophotometer (values in Table S4). BY08 and EAS13 formulations yield $\Delta[CO_3^{2-}]$ close to zero or negative, while the formulations of PAT15, SHA17, and SHA19 yield overall positive $\Delta[CO_3^{2-}]$, particularly PAT15. Regardless of the Pb(II) reagent, $\Delta[CO_3^{2-}]$ among the five approaches always distribute the same way: $\Delta[CO_3^{2-}]_{EAS13}$ and $\Delta[CO_3^{2-}]_{BY08}$ are comparable and usually show lower values than $\Delta[CO_3^{2-}]_{SHA17}$ and $\Delta[CO_3^{2-}]_{SHA19}$ that are also comparable, while $\Delta[CO_3^{2-}]_{PAT15}$ shows the highest positive values. In particular, one distinct feature between reagents is that *R* data obtained with $PbCl_2$ show larger dispersion and more outliers (red dots) than $Pb(ClO_4)_2$ data.

$\Delta[CO_3^{2-}]_{BY08}$ and $\Delta[CO_3^{2-}]_{EAS13}$ show mean values close to zero and mostly comprised within the ± 4 % limit for Atlantic Ocean cruises (CAIBOX, MOC2, OVIDE, RADPROF, RADCOR, and iFADO) and one Mediterranean Sea cruise (TALPRO) (Figure 2; Table S4), regardless of the Pb(II) reagent. Negative values beyond the ± 4 % limit are found for one cruise in the Atlantic Ocean (iFADO), two cruises in the Mediterranean Sea (HOTMIX and MSM72), and in regions influenced by Mediterranean waters (MEDWAVES), especially for $Pb(ClO_4)_2$ data (Figure 2; Table S4).

Clearly, $\Delta[CO_3^{2-}]_{PAT15}$ shows the largest positive values, mostly above the ± 10 % limit for data from either Pb(II) reagent, except for the MEDWAVES cruise that shows $\Delta[CO_3^{2-}]_{PAT15}$ centered around zero (Figure 2; Table S4). $\Delta[CO_3^{2-}]_{SHA17}$ and $\Delta[CO_3^{2-}]_{SHA19}$ yield mainly positive values between the ± 4 % and ± 10 % limits (Table S4). The SHA17 and SHA19 approaches overall show comparable results, which is expected since all the measurements were performed at 25 °C. These results support the consistency between the SHA17 and SHA19 approaches when the measurements are performed at the same temperature, and differences between them might be due to biases from the reference temperature during analysis (section 2.1), which can be accounted for with the SHA19 approach.

The approaches of SHA17 and SHA19 propose a correction (eq 5) to account for wavelength inaccuracies in the spectrophotometer. In this regard, $\Delta[CO_3^{2-}]_{SHA17}$ and $\Delta[CO_3^{2-}]_{SHA19}$ from measurements obtained with the SHI2600 spectrophotometer (HOTMIX, MSM72, RADPROF, RADCOR, and iFADO) showed positive values that decreased and approached zero after applying the measured $\Delta\lambda_{241.1}$ term for data from either Pb(II) reagent (Figure 2). However, Figure 2 shows that final readjusted $\Delta[CO_3^{2-}]_{SHA17}$ and $\Delta[CO_3^{2-}]_{SHA19}$ do not center completely around zero for some of these cruises (HOTMIX, RADPROF, and RADCOR). The PE850 spectrophotometer could only be examined during iFADO, for which $\Delta\lambda_{241.1}$ was zero, and corresponding $\Delta[CO_3^{2-}]_{SHA17}$ and $\Delta[CO_3^{2-}]_{SHA19}$ are well centered around zero only for data measured with $Pb(ClO_4)_2$ (Figure 2; Table S4). The $\Delta[CO_3^{2-}]$ for the cruises for which the $\Delta\lambda_{241.1}$ term could not be measured (CAIBOX, MOC2, OVIDE, TALPRO, and MEDWAVES) approached zero if *R* was readjusted using a $\Delta\lambda_{241.1}$ value of about 0.3 nm (results not shown).

3.2. Patterns in $\Delta[CO_3^{2-}]$ versus $[CO_3^{2-}]_{calc}$. The magnitude of $\Delta[CO_3^{2-}]$ is proportional to $[CO_3^{2-}]_{calc}$ itself,

https://doi.org/10.1021/acs.est.1c06083
Environ. Sci. Technol. 2022, 56, 7381−7395

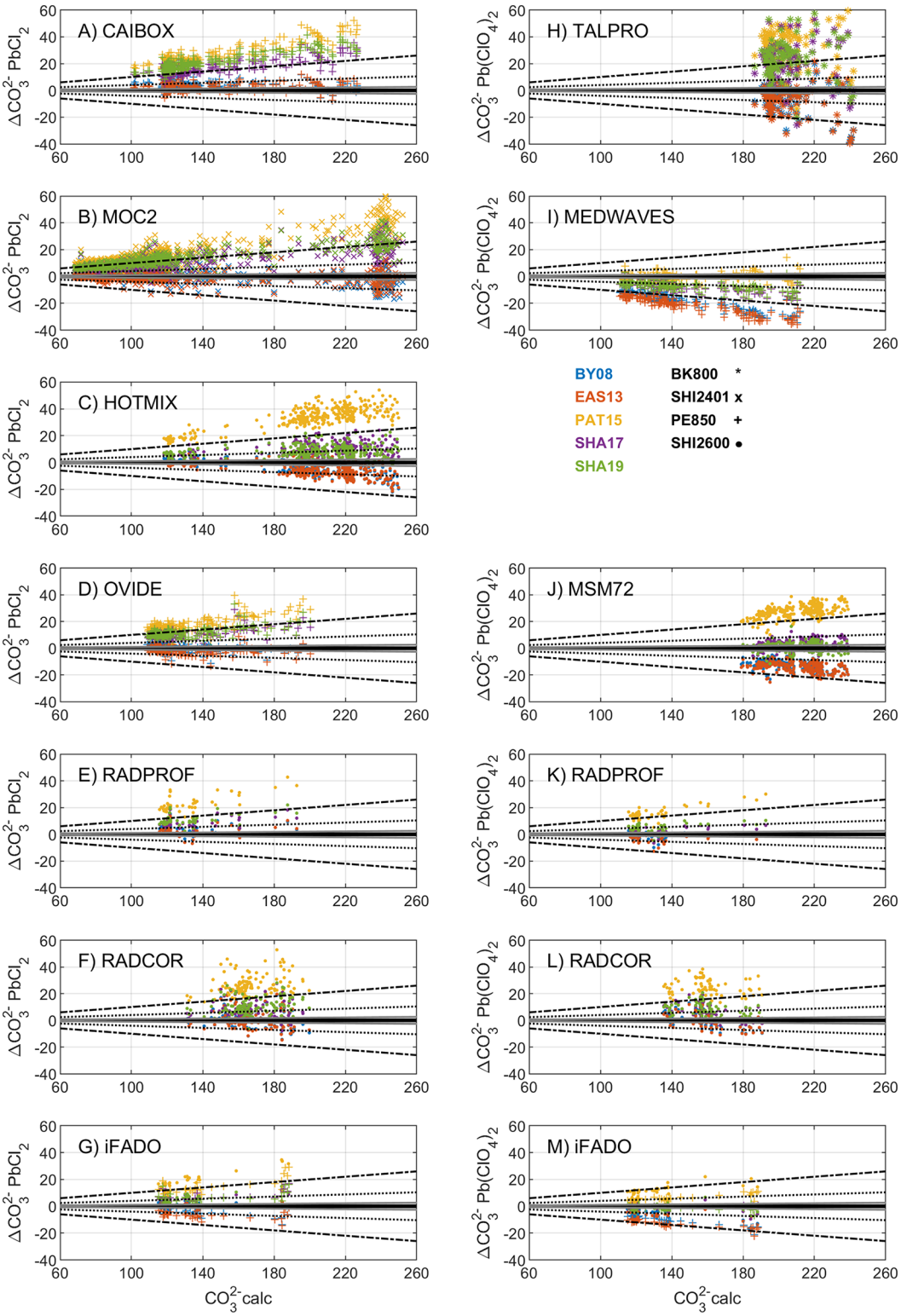

Figure 3. Spectrophotometric minus calculated carbonate ion content ($\Delta[CO_3^{2-}] = [CO_3^{2-}]_{spec} - [CO_3^{2-}]_{calc}$; in $\mu mol \cdot kg^{-1}$) as a function of $[CO_3^{2-}]_{calc}$ (calculated from pH-TA; $\mu mol \cdot kg^{-1}$) for each cruise (Figure 1; Table 1). $[CO_3^{2-}]_{spec}$ are obtained with five $[CO_3^{2-}]_{spec}$ formulations (Table S1) in color. Spectrophotometer models (Table S3) are identified with different symbols. Panels on the left and the right refer to $[CO_3^{2-}]_{spec}$ data measured with $PbCl_2$ and $Pb(ClO_4)_2$, respectively. $[CO_3^{2-}]_{calc}$ are reported at 25 °C and atmospheric pressure, except for SHA19 that are reported at the exact temperature of analysis. The SHA17 and SHA19 approaches include a wavelength correction ($\Delta\lambda_{241.1}$ = 0.2 nm; Table S1) for cruises where the SHI2600 was used (HOTMIX, MSM72, RADPROF, RADCOR, and iFADO; Table 1) and is null for the remaining cruises. Gray and dashed lines depict the GOA-ON relative standard uncertainty goals of ± 1 % for the climate-quality objective and ± 10 % for the weather-quality objective, respectively; the dotted line depicts the standard uncertainty limit of ± 4 % attributable to the internal consistency of the data set in this study.

https://doi.org/10.1021/acs.est.1c06083
Environ. Sci. Technol. 2022, 56, 7381−7395

as reported in all the works of the methodology,[24,25,28−30,44] regardless of the Pb(II) reagent, the spectrophotometer, or the approach used (Figure 3). The approaches by BY08 and EAS13 yield $\Delta[CO_3^{2-}]$ that mostly scatter around zero (CAIBOX, MOC2, and OVIDE) except for Mediterranean Sea cruises (i.e., high-salinity waters; HOTMIX, MSM72, MEDWAVES, and TALPRO) and for the iFADO cruise, where $\Delta[CO_3^{2-}]_{BY08}$ and $\Delta[CO_3^{2-}]_{EAS13}$ show negative values that decrease towards higher $[CO_3^{2-}]_{calc}$ (i.e., increasing $[CO_3^{2-}]_{spec}$ underestimation). The approaches by PAT15, SHA17, and SHA19 show the opposite $\Delta[CO_3^{2-}]$ patterns, with $\Delta[CO_3^{2-}]_{PAT15}$, $\Delta[CO_3^{2-}]_{SHA17}$, and $\Delta[CO_3^{2-}]_{SHA19}$ that increase proportionally to $[CO_3^{2-}]_{calc}$ (i.e., increasing $[CO_3^{2-}]_{spec}$ overestimation). Figure 3 shows that the same relative distribution among $\Delta[CO_3^{2-}]$ from each approach is observed for the whole $[CO_3^{2-}]_{calc}$ range, where $\Delta[CO_3^{2-}]_{EAS13} \approx \Delta[CO_3^{2-}]_{BY08} < \Delta[CO_3^{2-}]_{SHA17} \approx \Delta[CO_3^{2-}]_{SHA19} < \Delta[CO_3^{2-}]_{PAT15}$, as reported in section 3.1. This pattern between approaches was expected for the whole $[CO_3^{2-}]_{calc}$ range at salinity 35, as shown in Figure S2A. It is attributable to differences among calibration functions (Table S2) that are larger at low R values (i.e., higher $[CO_3^{2-}]_{calc}$; Figure S2) and higher salinities (Figure S3).

The spectrophotometer used affects the dispersion (Appendix C) in $\Delta[CO_3^{2-}]$ (Figure 3). For instance, data from the TALPRO cruise show larger $\Delta[CO_3^{2-}]$ dispersion and also larger whisker boxes than other cruises (Figure 2). During TALPRO, $[CO_3^{2-}]_{spec}$ values were measured with a BK800 spectrophotometer (Table 1), which is a single beam and also the least accurate spectrophotometer of all the models used in terms of photometric accuracy (Appendix C; Table S3). In contrast, cruises using the PE850 spectrophotometer (CAIBOX, MEDWAVES, OVIDE, and iFADO) show the lowest $\Delta[CO_3^{2-}]$ dispersion for the entire $[CO_3^{2-}]_{calc}$ range (Figure 3). This spectrophotometer has the best photometric accuracy and also a very low value for stray light (Table S3). Between them, in terms of photometric accuracy performance, the SHI2401 and SHI2600 models (Table S3) yield data with increasing dispersion toward higher $[CO_3^{2-}]_{calc}$ for cruises where $[CO_3^{2-}]_{calc} > 180\ \mu mol{\cdot}kg^{-1}$ (MOC2, HOTMIX, and MSM72). The larger dispersion for RADCOR over the entire $[CO_3^{2-}]_{calc}$ range might be related to being a coastal site with higher inherent variability.[7]

Also, the spectrophotometer used affects the overall bias (Appendix C) in $\Delta[CO_3^{2-}]$. PE850 exemplifies well that highly precise equipment in terms of dispersion (i.e., photometric accuracy; Table S3) can exhibit very different performance in terms of bias (i.e., wavelength accuracy; CAIBOX, MEDWAVES, OVIDE, and iFADO; Figure 3). In this regard, since $\Delta[CO_3^{2-}]$ from each of the five approaches always keep the same relationship among them, the approaches that respectively show the most internally consistent $\Delta[CO_3^{2-}]$, within the ± 4 % limit of $[CO_3^{2-}]_{calc}$, are cruise-dependent, in relation to the spectrophotometer bias: SHA17 and SHA19 (MSM72, $Pb(ClO_4)_2$; iFADO, both reagents), EAS13 and BY08 (CAIBOX, MOC2, and OVIDE, all using $PbCl_2$; RADPROF and RADCOR, both reagents), and PAT15 (MEDWAVES, $Pb(ClO_4)_2$).

3.3. Limits of Consistency for $\Delta[CO_3^{2-}]$. No approach fulfills the GOA-ON relative standard uncertainty goal of ± 1 % for the climate-quality objective, but most results, except those obtained with the PAT15 approach, meet the weather-quality objective of ± 10 % uncertainty for any range of $[CO_3^{2-}]_{calc}$ (Figure 3; Table S5).

Cruises in the Atlantic Ocean, except the iFADO cruise, show $\Delta[CO_3^{2-}]$ values within ± 4 % uncertainty with the BY08 and EAS13 approaches for the whole $[CO_3^{2-}]_{calc}$ range (Figure 3; Table S5). Hence, $[CO_3^{2-}]_{specBY08}$ or $[CO_3^{2-}]_{specEAS13}$ are internally consistent within the assumed uncertainty (Section 2.2). This was already reported by Fajar et al.[44] for the Atlantic Ocean data (CAIBOX, MOC2, and OVIDE). Although the EAS13 approach was reported to be accurate enough (± 2 %) only below 180 $\mu mol{\cdot}kg^{-1}$ by PAT15,[29] the results in this study suggest that both BY08 and EAS13 formulations determine consistent $[CO_3^{2-}]_{spec}$ (± 4 %) in the North Atlantic Ocean, over the 68 $\mu mol{\cdot}kg^{-1}$ − 252 $\mu mol{\cdot}kg^{-1}$ range.

For high-salinity waters, the BY08 and EAS13 approaches yield mostly negative $\Delta[CO_3^{2-}]$ (although still within ± 4 % when using $PbCl_2$ (HOTMIX)) that show larger $\Delta[CO_3^{2-}]$ (within ±10 % or beyond) when using $Pb(ClO_4)_2$ (TALPRO, MEDWAVES, and MSM72; Table S5). The EAS13 approach was reported to underestimate $[CO_3^{2-}]_{spec}$ at salinity > 36, $[CO_3^{2-}]_{calc} > 150\ \mu mol{\cdot}kg^{-1}$, and high pH.[28,44] This study shows that the underestimation of $[CO_3^{2-}]_{spec}$ occurs for the HOTMIX, MEDWAVES, and MSM72 cruises, with the BY08 and EAS13 approaches. In this regard, EAS13 suggested that the Pb(II) complexation model should be extended to include the formation of other potential Pb(II) complexes to address the trend in the residuals seen at high $[CO_3^{2-}]$ (Appendix B). However, opposite to the approaches of BY08 and EAS13, the most recent approaches of SHA17 and SHA19, with the latter covering a wide salinity fitting range (Table S1), do not underestimate $[CO_3^{2-}]_{spec}$; yet, in some cruises overestimate it (Figure 3; Table S5). Hence, the hypothesis of a mischaracterization of the Pb(II) complexation in high-salinity and high-pH waters would not be supported. Instead, the fitting procedure for the terms in eq 1 for each approach might cause the observed negative $\Delta[CO_3^{2-}]$, as the greatest changes regarding the stability constant for the formation of the $PbCO_3$ complex (Figure S2B) and the terms $\left[\frac{1}{R-e_1}\right]$ and $\left[1 - R{\cdot}\frac{e_3}{e_2}\right]$ (Figure S3) were mostly generated for high-salinity and low R values.

4. DISCUSSION

Both the observed mean $\Delta[CO_3^{2-}]$ values and corresponding trends versus $[CO_3^{2-}]_{calc}$, taking into account reagents, equipment specifications and calibration, salinity ranges, and $[CO_3^{2-}]_{calc}$, suggest that the method is inconsistent among approaches with regard to its performance for $[CO_3^{2-}]_{spec}$ measurement. In this section, the methodological changes among approaches are assessed to identify the factors that explain the observed differences in $\Delta[CO_3^{2-}]$.

4.1. Random and Systematic Uncertainty of the Absorbance Ratio (R): Precision and Accuracy of Absorbance Measurements. Since R values are inversely proportional to $[CO_3^{2-}]_{spec}$ (i.e., lower R values yield higher $[CO_3^{2-}]_{spec}$; Figure S2A inset), the assessment of $[CO_3^{2-}]_{spec}$ is less precise at a higher $[CO_3^{2-}]$, and this is independent of the equipment or approach used. Within R (eq 2), ${}_{250}A$ varies substantially with pH,[24,27,33] becoming lower as $[CO_3^{2-}]$ increases, while ${}_{234}A$ is always higher, lying close to the isosbestic point (Appendix C) and is thus less sensitive to changes in $[CO_3^{2-}]$. In consequence, lower R values will inherently have larger random uncertainty, or lower precision, which translates into a fan-shape distribution of $\Delta[CO_3^{2-}]$ for results obtained with any approach, particularly at $[CO_3^{2-}]_{calc} > 180\ \mu mol{\cdot}kg^{-1}$ (Figure 3). This fact, derived from R being a ratio of absorbances

https://doi.org/10.1021/acs.est.1c06083
Environ. Sci. Technol. 2022, 56, 7381−7395

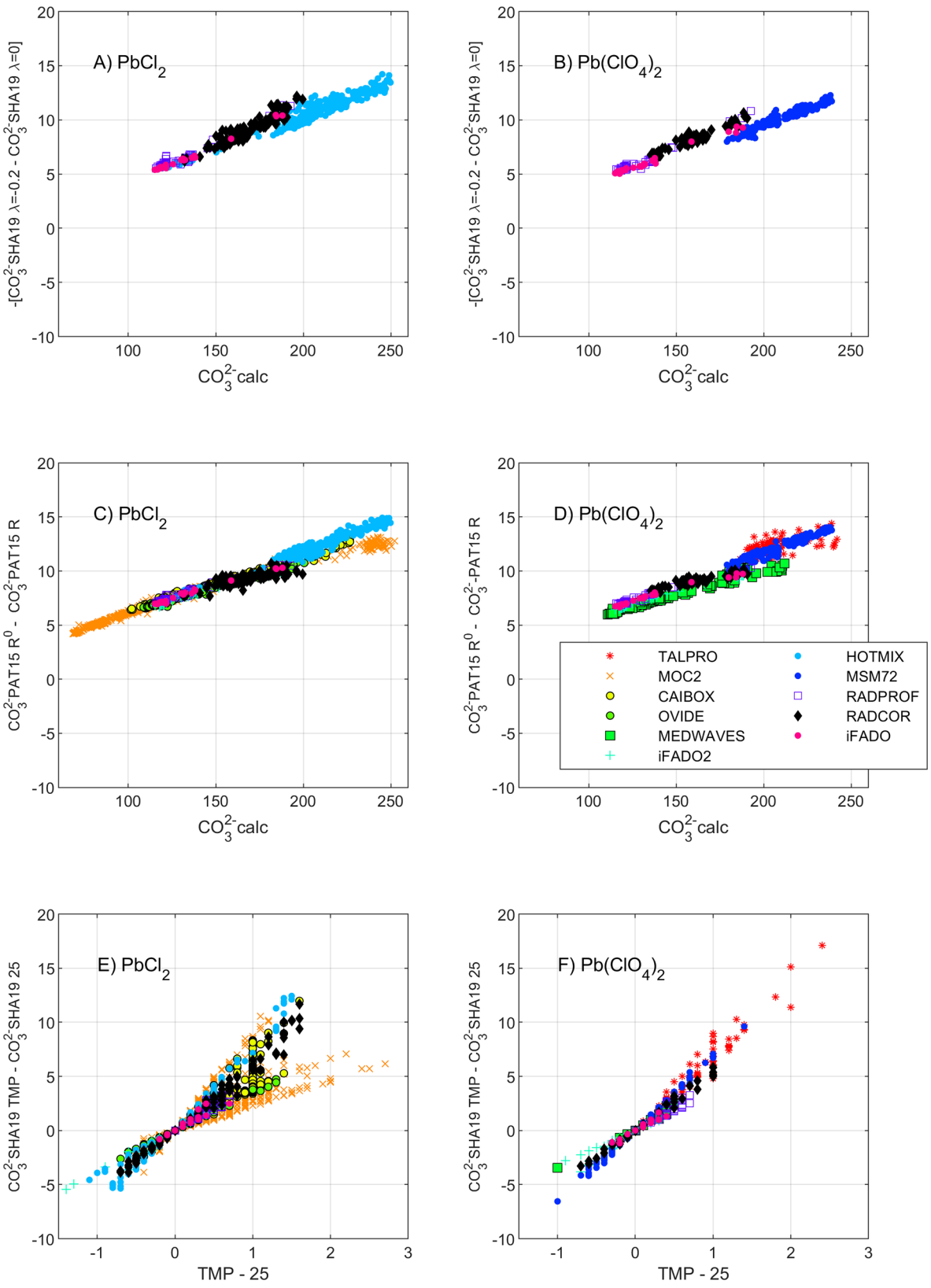

Figure 4. Effect on $[CO_3^{2-}]_{spec}$ (in μmol·kg^{-1}) of (A and B) the wavelength offset correction proposed by SHA17 as a function of $[CO_3^{2-}]_{calc}$ (calculated from TA-pH; μmol·kg^{-1}), (C and D) the Pb(II) reagent perturbation correction according to PAT15 as a function of $[CO_3^{2-}]_{calc}$, and (E and F) the functions proposed by SHA19 as a function of the temperature bias regarding 25 °C. Differences are calculated as (A and B) $[CO_3^{2-}]_{spec}$ calculated using a wavelength offset correction ($\Delta\lambda_{241.1}$) of 0.2 nm (eq 4) minus $[CO_3^{2-}]_{spec}$ obtained without correction, for cruises using the SHI2600 spectrophotometer; (C and D) $[CO_3^{2-}]_{spec}$ calculated with the corrected minus the original Pb(II) absorbance ratio (R^0 and R, respectively; Table S1); (E and F) $[CO_3^{2-}]_{spec}$ at the real temperature (TMP) of analysis minus $[CO_3^{2-}]_{spec}$ at 25 °C. Data measured with $PbCl_2$ or $Pb(ClO_4)_2$ are shown on the left and the right panels, respectively. All panels share the same legend.

https://doi.org/10.1021/acs.est.1c06083
Environ. Sci. Technol. 2022, 56, 7381−7395

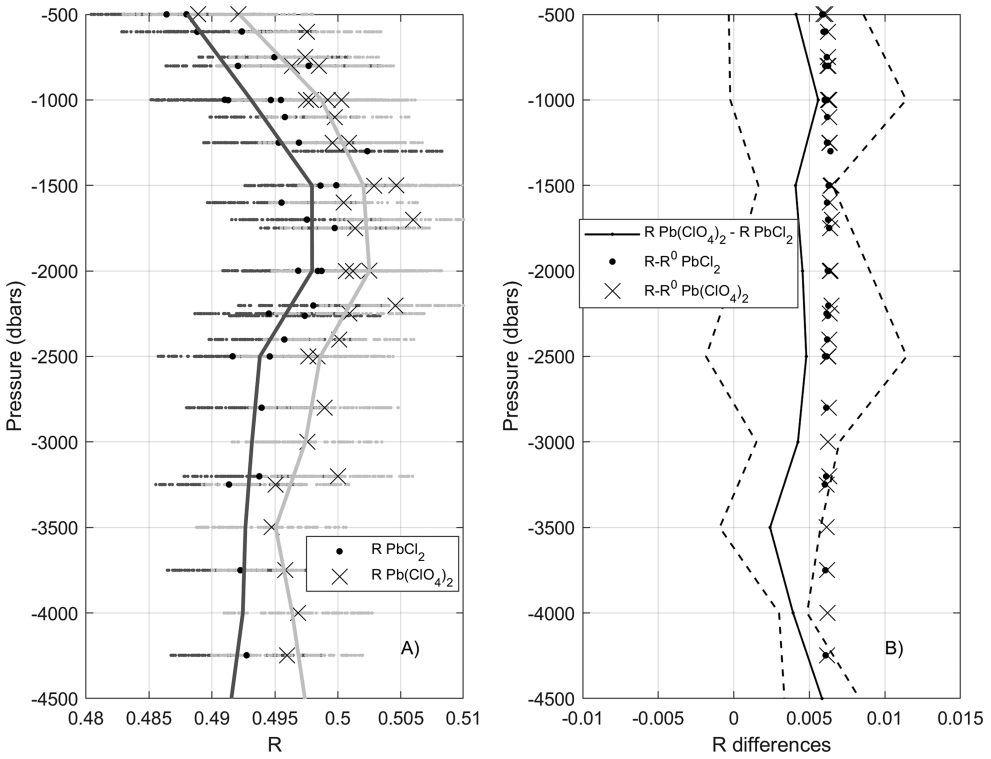

Figure 5. (A) Mean profiles of Pb(II) absorbance ratios (R) for sample replicates measured with $PbCl_2$ (dark line and dots) and $Pb(ClO_4)_2$ (gray line and crosses) during the RADPROF cruise (Table 1). Horizontal dotted lines accompanying each R value correspond to a Monte Carlo perturbation analysis introducing a random uncertainty within ± 0.006 in measured R values according to SHI2600 specifications (Table S3). (B) Mean difference profile of R measured with $Pb(ClO_4)_2$ minus R measured with $PbCl_2$ (solid line) and corresponding uncertainty (dashed lines) calculated considering the Monte Carlo perturbed R results shown in panel A. Additionally, the value of the R perturbation correction according to PAT15 ($R^0 - R$; Table S1), for RADPROF replicate measurements with $PbCl_2$ (dark dots) and $Pb(ClO_4)_2$ (gray crosses) is also depicted. The sign of the perturbation values has been reversed for representation purposes.

with dissimilar magnitudes, can be empirically evidenced using a Monte Carlo analysis (Appendix E; Figure S5).

Technical specifications of the spectrophotometer regarding the photometric and wavelength accuracies, and the stray light (Table S3) might be critical for setting the mean $\Delta[CO_3^{2-}]$ value and its relationship to $[CO_3^{2-}]_{calc}$. In this study, the spectrophotometers used have variable values for photometric accuracy (Appendix C), which translates into variable R uncertainty (Table S3) that will affect $\Delta[CO_3^{2-}]$ to a different extent but always cause the same distribution (Figure S5). A spectrophotometer with low photometric accuracy will introduce more random noise in R measurements, especially at low R values, resulting in even more dispersed $\Delta[CO_3^{2-}]$ at high $[CO_3^{2-}]$. Another factor affecting random uncertainty might be the stray light of the spectrophotometer (Appendix C). By combining both random sources of uncertainty and according to the spectrophotometers specifications (Table S3), the spectrophotometer models could be ordered from the highest to the lowest expected precision as PE850, SHI2600, SHI2401, and BK800, which agrees with the observed results (Figure 3; Tables S4 and S5).

While random uncertainty in R explains the larger dispersion of $\Delta[CO_3^{2-}]$ at high $[CO_3^{2-}]$, it does not explain systematic biases in $\Delta[CO_3^{2-}]$ toward positive or negative values outside the ± 4 % limit (Figure 3). The wavelength accuracy is critical in this regard (Appendix C) since it could be significant when measuring ${}_{250}A$, located on a slope, where small variations in wavelength cause significant changes in ${}_{250}A$, and to a lesser extent in ${}_{234}A$, located near a peak. This was accounted for in SHA17, who proposed a wavelength offset term ($\Delta\lambda_{241.1}$; eq 5) to correct inaccuracies in the equipment wavelength calibration.

In this regard, measuring the holmium oxide standard to assess $\Delta\lambda_{241.1}$ for the SHI2600 spectrophotometer was not simple. The $\Delta\lambda_{241.1}$ term is supposed to remain constant as long as the equipment is not recalibrated.[30] However, 15 $\Delta\lambda_{241.1}$ measurements were averaged to obtain a stable value (section 2.1). Our experience quantifying $\Delta\lambda_{241.1}$ indicates that (i) according to SHA17, shifts in $\Delta\lambda_{241.1}$ on the order of 0.05 nm are supposed to be significant, which would imply that the holmium standard should be measured each time that the spectrophotometer is used, not only when recalibrated, because differences of this order were found for measurements of the same holmium oxide standard in different measurement exercises; (ii) the average $\Delta\lambda_{241.1}$ found for SHI2600 (0.20 nm ± 0.06 nm) is lower than the wavelength accuracy of the spectrophotometer (± 0.3 nm; Table S3), and (iii) the average $\Delta\lambda_{241.1}$ equals the uncertainty of the certified holmium peak position (241.15 nm ± 0.20 nm). Therefore, R measurements are likely corrected over the limits of the SHI2600 spectrophotometer and holmium standard specifications. However, when the offset correction is applied, $\Delta[CO_3^{2-}]_{SHA19}$ decrease proportionally to $[CO_3^{2-}]_{calc}$ by about 5 μmol·kg^{-1} to 14 μmol·kg^{-1}, for measurements with both reagents (Figure 4A, B). The SHA19 approach also uses $\Delta\lambda_{241.1}$. Despite adding complexity to the analysis procedure, both $\Delta[CO_3^{2-}]_{SHA17}$ and $\Delta[CO_3^{2-}]_{SHA19}$ meet the ± 4 % uncertainty limit (Tables S3 and S4) and can be considered internally consistent, when the $\Delta\lambda_{241.1}$ term is assessed, with the HOTMIX and RADCOR exceptions.

https://doi.org/10.1021/acs.est.1c06083
Environ. Sci. Technol. 2022, 56, 7381−7395

Technical specifications of the spectrophotometer seem crucial for precise and accurate R measurements. Most equipment might not achieve the accuracy necessary for $[CO_3^{2-}]_{spec}$ determination (Table S3), including the model UV8453 used for describing the methodology (Table 1).[30] An accurate quantification of e_3/e_2 and the fitting of $\frac{^{CO_3}\beta_1}{e_2}$ and e_1 in eq 1 would benefit from using the best equipment in terms of technical specifications.

4.2. Change in Pb(II) Reagent and Double Addition Correction. PAT15 proposed a change in the Pb(II) reagent, from $PbCl_2$ to $Pb(ClO_4)_2$, doubling the final Pb(II) concentration in the cuvette (Table S1), to increase the signal-to-noise ratio of the absorbance measurements. Additionally, the authors proposed an R perturbation correction (eq 4) that enlarges the resulting $[CO_3^{2-}]_{specPAT15}$ proportionally to $[CO_3^{2-}]_{calc}$ by 5 μmol·kg^{-1} to 15 μmol·kg^{-1} with regard to uncorrected R values (Figure 4C, D). As a result, $\Delta[CO_3^{2-}]_{PAT15}$ values reach 20 μmol·kg^{-1} − 40 μmol·kg^{-1} at higher $[CO_3^{2-}]_{calc}$ (Figure 3). If the correction is not applied, $\Delta[CO_3^{2-}]_{PAT15}$ compares well with $\Delta[CO_3^{2-}]_{SHA17}$ and $\Delta[CO_3^{2-}]_{SHA19}$ (data not shown), which confirms that the large positive $\Delta[CO_3^{2-}]_{PAT15}$ values are mainly caused by the perturbation correction. In this regard, no R perturbation correction was reported by BY08 or EAS13 for $PbCl_2$ since the Pb(II) concentration in the cuvette (7.5 μmol·L^{-1}; Table S1) does not induce significant sample perturbation.[28] Neither of the most recent procedures by SHA17 and SHA19 recommends using a perturbation correction for R values measured with $Pb(ClO_4)_2$.

During the RADPROF cruise, R values were measured on replicate samples with $PbCl_2$ and $Pb(ClO_4)_2$ with the SHI2600 spectrophotometer (Table 1). The same comparison experiment was repeated during the iFADO cruise, where two different spectrophotometers were used: SHI2600 and PE850 (Table 1). RADPROF results reveal that R values measured with $Pb(ClO_4)_2$ are higher than those measured with $PbCl_2$ (Figure 5A) for sample replicates. The difference is almost constant for the whole depth profile and amounts to 0.0044 ± 0.0010 ($Pb(ClO_4)_2$ − $PbCl_2$; Figure 5B). Noticeably, the two reagents might behave differently characterizing the Pb(II) absorbance signal for the same seawater conditions. Considering a random uncertainty of ± 0.006 (Table S3) in R measurements, according to SHI2600 specifications, the mean R difference found between reagents is close to the R random uncertainty. In this regard, a Monte Carlo experiment introducing this random noise in the bulk R data from both reagents shows that resulting R values overlap (Figure 5A). This overlapping is magnified for spectrophotometers with lower photometric accuracy (data not shown). This would explain the absence of a significant difference of mean $\Delta[CO_3^{2-}]$ using either reagent and formulations (Figure 2 and Table S4). In addition, Figure 5B shows that the observed R difference between reagents has almost the same magnitude but opposite sign to the magnitude of the R perturbation correction proposed by PAT15 (−0.006 ± 0.0005) for data measured using $PbCl_2$ or $Pb(ClO_4)_2$. During the iFADO cruise, the same overall results were observed for both the SHI2600 and PE850 spectrophotometers: R differences between reagents ($Pb(ClO_4)_2$ − $PbCl_2$) were 0.0050 ± 0.0015 and 0.0061 ± 0.0006, respectively (data not shown). In this regard, the possibility that perchlorate (ClO_4^-) could be absorbing light at the target wavelengths was examined using a solution of ClO_4^- (>98% purity) in different seawater conditions in terms of salinity and $[CO_3^{2-}]_{calc}$, showing that measured absorbances were not different from zero at the target wavelengths (results not shown).

During the iFADO cruise, further comparison experiments of reagents and spectrophotometers were performed on quadruplicate samples through scan measurements (Appendix F). The observed results show that $_{234}A$ and $_{250}A$ are always higher when measured using $Pb(ClO_4)_2$ compared to $PbCl_2$ (Figure S6), which is expected considering that the final Pb(II) concentration in the cuvette is higher when using $Pb(ClO_4)_2$ (Table S1). $_{234}A$ and $_{250}A$ measurements obtained with different spectrophotometers are broadly coincident for data measured with $PbCl_2$ (Figure S6A,B), which is also the case for $_{250}A$ data measured with $Pb(ClO_4)_2$ (Figure S6D). While a good agreement was observed between the SHI2600 and PE850 spectrophotometers for the measurements of $_{234}A$ and $_{250}A$ using $PbCl_2$ (Figure S6A,B), only measurements of $_{250}A$ agreed between the two instruments when $Pb(ClO_4)_2$ was used (Figure S6D). In fact, $_{234}A$ values measured with $Pb(ClO_4)_2$ clearly deviate from the 1:1 line, with SHI2600 yielding higher values than PE850 (Figure S6C). These results are well depicted in Figure S7A, showing the overlapping of $_{250}A$ versus $_{234}A$ measured with $PbCl_2$ for both spectrophotometers. However, Figure S7B also shows that $Pb(ClO_4)_2$ data split into two groups depending on the spectrophotometer used. Consequently, R values from $PbCl_2$ are comparable between SHI2600 and PE850, but PE850 yields higher R values when using $Pb(ClO_4)_2$ (Figure S7C).

The observed results are surprising as larger differences in the $_{250}A$ value were expected because it is located in a slope area. No sampling, preservation, or manipulation differences between replicates can be ascribed to the observed results. Considering the similar technical specifications between SHI2600 and PE850 in terms of wavelength and photometric accuracy (Table S3), and the fact that mean $_{234}A$ and $_{250}A$ integrate absorbance data around ± 2 nm of the target wavelengths (Appendix F), the only difference between them is the stray light specification (Appendix C). However, this would lead to $_{234}A$ PE850 > $_{234}A$ SHI2600, which is opposite to the observed results.

In conclusion, the change in Pb(II) reagent seems to affect the determination of $[CO_3^{2-}]_{spec}$. Using $Pb(ClO_4)_2$ improves data dispersion (Figure 2) regarding $PbCl_2$, but $Pb(ClO_4)_2$ also appears to be more sensitive to inaccuracies in the absorbance signal related to the technical specifications of the equipment.

4.3. In Situ Temperature Correction. The approaches by BY08, EAS13, PAT15, and SHA17 need temperature control at 25 °C ± 0.05 °C (Table S1), while SHA19 introduced temperature-dependent terms in the absorptivity coefficients and in the formation constant (Table S2) that allow determinations over a range of temperatures (3 °C < t ± 0.05 °C < 40 °C; Table S1). Recall that Soli et al.[31] reported that the formation constant (eq S3) is almost constant for the range 15−35 °C. This is reflected in Table S2 where the temperature dependence of the formation constant is minor, while the absorptivity terms have stronger temperature dependence. SHA19 reported an error of about 3% in measured $[CO_3^{2-}]_{specSHA19}$ for 1 °C bias in temperature. Using the SHA19 approach and the temperature recordings for each sample, the observed bias in $[CO_3^{2-}]_{spec}$ for samples that lacked temperature control at 25 °C (Figure 4E, F) is in agreement with the bias reported by SHA19. Hence, $[CO_3^{2-}]_{spec}$ is underestimated in samples with a temperature higher than 25 °C that are incorrectly reported at 25 °C, underestimating $[CO_3^{2-}]_{spec}$ by about 5 μmol·kg^{-1} (≈ 3%) for 1 °C positive bias in

https://doi.org/10.1021/acs.est.1c06083
Environ. Sci. Technol. 2022, 56, 7381−7395

temperature. All the approaches recommend temperature control within ± 0.05 °C (Table S1), and the results of this study suggest that temperature control is needed at least within ± 1 °C to reduce uncertainty within the ± 4 % limit.

5. CONCLUSIONS

The assessment of the internal consistency between $[CO_3^{2-}]_{spec}$ from the five different approaches of the methodology and $[CO_3^{2-}]_{calc}$ according to data in this study allowed a detailed comparison of the differential factors among the evolving approaches studied, regarding the respective sets of calibration functions to infer $[CO_3^{2-}]_{spec}$ (Table S2) as well as an examination of other methodological updates proposed through time (Table S1). Overall results suggest that further documentation is needed until $[CO_3^{2-}]_{spec}$ can be implemented as the fifth measurable variable of the seawater CO_2 system. A summary of areas where improvement is needed to enhance the long-term reproducibility of $[CO_3^{2-}]_{spec}$ to warrant the broader implementation of $[CO_3^{2-}]_{spec}$ measurements are detailed in the following:

(i) Current robustness of $[CO_3^{2-}]_{spec}$ for OA monitoring studies. $[CO_3^{2-}]_{spec}$ observations reported in this study suggest that approaches of the methodology assessed (BY08, EAS13, PAT15, SHA17, and SHA19; Table S1) are not yet ready for applications that require climate-quality measurements because they do not meet the GOA-ON objective of ± 1 % standard uncertainty for the whole studied range of $[CO_3^{2-}]_{calc}$. Moreover, none of the five approaches assessed is clearly the best option for being globally implemented. But all the approaches except PAT15 fulfill the weather-quality standard of ± 10 %. Those approaches proven to meet the weather-quality objective could be used and further tested in studies facing large temporal or spatial variability in $[CO_3^{2-}]$ or in other compatible applications like OA experimentation in aquaria, shellfish aquaculture, or coastal conservation.

(ii) $[CO_3^{2-}]_{spec}$ as the fifth CO_2 measurable variable and internal consistency analysis of CO_2 overdetermined systems. Few $[CO_3^{2-}]_{spec}$ observations reported in this study meet the expected ± 2 % standard uncertainty attained in reference bibliography (Table S1). Furthermore, the relative $\Delta[CO_3^{2-}]$ distribution between approaches remains the same for the entire salinity and $[CO_3^{2-}]_{calc}$ ranges studied, where $[CO_3^{2-}]_{specBY08} \approx [CO_3^{2-}]_{specEAS13} < [CO_3^{2-}]_{specSHA17} \approx [CO_3^{2-}]_{specSHA19} < [CO_3^{2-}]_{specPAT15}$ but demonstrates an overall lack of consistency between them. This implies that using diverse R data sets with newer algorithms does not guarantee an improvement in the recalculated data set, which is particularly unfavorable for the maintenance of time-series. Time-series or data sets tracking the $[CO_3^{2-}]_{spec}$ methodological evolution (Table S1) would lack consistency between results obtained with former procedures (BY08 and EAS13) with regard to the most recent approaches from SHA17, SHA19, and PAT15. According to these findings, it might not be recommendable to include $[CO_3^{2-}]_{spec}$ as the fifth CO_2 measurable variable until the methodology is extensively reviewed and implemented by more research groups. There are few references from independent groups reporting the use of the $[CO_3^{2-}]_{spec}$ methodology,[44] which is a clear disadvantage for its widespread implementation as a well-tested method. This point was considered in the GLODAPv2.2020 update where no $[CO_3^{2-}]$ data were included.[36] The inclusion of $[CO_3^{2-}]_{spec}$ as the fifth measurable variable with any of the approaches for internal consistency studies would likely add noise in the already complicated seawater CO_2 system modeling and characterization, where known inconsistencies are currently under debate.[38,51] Additionally, caution is needed when pairing $[CO_3^{2-}]_{spec}$ with another seawater CO_2 variable to estimate the whole seawater CO_2 system.[25] According to the observed results, a standard uncertainty larger than 2 % should be assigned to $[CO_3^{2-}]_{spec}$ to evaluate propagated uncertainties in derived CO_2 variables.

(iii) SOP for $[CO_3^{2-}]_{spec}$ measurements and factors to be further specified. This study highlights several inconsistencies in the $[CO_3^{2-}]_{spec}$ methodology evolution related to the Pb(II) reagent, the equipment specifications, and controversial perturbation and wavelength offset corrections, which points to the need to provide a well-described SOP for end-users, as available for the other four seawater CO_2 system variables[17] that allows the successful performance of the method in diverse seawater conditions. A summary of likely significant factors that should be revisited and made clearer to users follows.

5.1. Spectrophotometer. The technical specifications regarding photometric and wavelength accuracies and the stray light seem crucial for $[CO_3^{2-}]_{spec}$ determination. The observed $\Delta[CO_3^{2-}]$ values reflect the dependence between the degree of data dispersion and the photometric accuracy of the spectrophotometer. The stray light seems to cause significant differences in ${}_{234}A$ between spectrophotometers when $Pb(ClO_4)_2$ is used, but the reason is unknown. Additionally, the use of this reagent demands the assessment of an offset correction ($\Delta\lambda_{241.1}$; Table S1) related to the wavelength accuracy of the equipment to correct systematic biases in the data. However, $\Delta\lambda_{241.1}$ assessment and implementation should be described more clearly since it seems controversial, going beyond the limits of uncertainty of both the wavelength accuracy specifications of the spectrophotometers and the holmium oxide certified standard accuracy.

5.2. Pb(II) Reagent. R values obtained with $Pb(ClO_4)_2$ are about 0.004−0.006 units higher than R measured with $PbCl_2$. Such difference seems insignificant when introduced in the formulations of the different approaches for calculating $[CO_3^{2-}]_{spec}$. In this regard, $\Delta[CO_3^{2-}]$ showed less dispersion for data measured with $Pb(ClO_4)_2$, which would support the reagent change. Nevertheless, $Pb(ClO_4)_2$ might cause the ${}_{234}A$ characterization to become more sensitive to the spectrophotometer specifications, thus impacting R measurements to a larger extent than when using $PbCl_2$. Differences in R values measured with the two Pb(II) reagents should be assessed to ensure the production of consistent data sets between groups and in time.

5.3. Temperature Sensitivity. Temperature control is needed within ± 0.05 °C to obtain $[CO_3^{2-}]_{spec}$ as accurate as possible within the capabilities of the methodology or at least within ± 1 °C to keep the uncertainty within the ± 4 % limit attributable to internal consistency.

5.4. Ranges of Salinity and pH Validity. The salinity ranges assessed to fit the various sets of calibration functions might impact the accuracy of the resulting $[CO_3^{2-}]_{spec}$ and the

https://doi.org/10.1021/acs.est.1c06083
Environ. Sci. Technol. 2022, 56, 7381−7395

applicability of a given approach. Valid salinity ranges for the BY08 and EAS13 approaches comprise the Atlantic Ocean but not high-salinity waters ($S > 36.5$) where they underestimate $[CO_3^{2-}]_{spec}$. Overestimation of $[CO_3^{2-}]_{spec}$ is observed, for both the Atlantic Ocean and the Mediterranean Sea with the approaches of PAT15, SHA17, and SHA19. The approaches of BY08 and SHA19 characterized the calibration functions for large salinity ranges: $20 < S < 36$ and $20 < S < 40$, respectively (Table S1). However, these salinity ranges were reached through modification of natural seawater in the laboratory. In BY08 all data was experimental, while in SHA19 they used data from natural samples but merged them with experimental data with broader salinity conditions. The salinity range assessed with natural seawater samples for characterizing the sets of calibration functions is shorter: $26.6 < S < 36.72$, among approaches (Table S1). Although the five sets of calibration functions showed the lowest $[CO_3^{2-}]_{spec}$ uncertainties at the lower ranges of $[CO_3^{2-}]_{calc}$ (Figures 3 and S5), suggesting that this would likely apply for seawater at lower salinities than the lowest ranges in this study (i.e., $S < 33.7$), observational evidence is needed to confirm this. Further $[CO_3^{2-}]_{spec}$ observations are also recommendable for high-salinity waters. Ideally, a reevaluation of the calibration functions should be performed using only data from natural seawater samples.

The existence of five approaches that show inconsistencies among them discourages widespread $[CO_3^{2-}]_{spec}$ determination. The ocean CO_2 community would benefit from an SOP and the availability of CRMs for $[CO_3^{2-}]_{spec}$ measurement. The SOP should include well-described and validated best practices to be implemented unambiguously by other users interested in setting up $[CO_3^{2-}]_{spec}$ measurements.

■ ASSOCIATED CONTENT

Supporting Information

The Supporting Information is available free of charge at https://pubs.acs.org/doi/10.1021/acs.est.1c06083.

Appendixes showing (A) Global ocean distribution of carbonate ion content and saturation states. Figure S1. (B) Evolution of the methodology for measuring carbonate ion content, Figures S2 and S3 and Tables S1 and S2. (C) Terminology, Table S3. (D) $\Delta[CO_3^{2-}]$ uncertainty assessment: uncertainty in $[CO_3^{2-}]_{calc}$ estimation, Figure S4 and Tables S4 and S5. (E) $\Delta[CO_3^{2-}]$ uncertainty assessment: $[CO_3^{2-}]_{spec}$ uncertainty related to the absorbance ratio. Monte Carlo analysis, Figure S5. (F) $\Delta[CO_3^{2-}]$ uncertainty assessment: $[CO_3^{2-}]_{spec}$ uncertainty related to the absorbance ratio. Absorbance measurements with both Pb(II) reagents and different spectrophotometers, Figures S6 and S7 (PDF)

■ AUTHOR INFORMATION

Corresponding Author

Elisa F. Guallart − *Centro Oceanográfico de A Coruña (COAC-IEO), CSIC, DC 15001 A Coruña, Spain; Institut de Ciències del Mar (ICM), CSIC, DC 08003 Barcelona, Spain;* orcid.org/0000-0003-2965-6671; Phone: (+34) 932309500; Email: efguallart@icm.csic.es; Fax: (+34) 932309555

Authors

Noelia M. Fajar − *Centro Oceanográfico de A Coruña (COAC-IEO), CSIC, DC 15001 A Coruña, Spain; Instituto de Investigacións Mariñas (IIM), CSIC, DC 36208 Vigo, Spain*

Maribel I. García-Ibáñez − *School of Environmental Sciences, University of East Anglia (UEA), Norwich NR47TJ, United Kingdom; Institut de Ciències del Mar (ICM), CSIC, DC 08003 Barcelona, Spain;* orcid.org/0000-0001-5218-0064

Mónica Castaño-Carrera − *Centro Oceanográfico de A Coruña (COAC-IEO), CSIC, DC 15001 A Coruña, Spain*

Rocío Santiago-Doménech − *Centro Oceanográfico de Baleares (COB-IEO), CSIC, DC 07015 Palma de Mallorca, Balearic Islands, Spain*

Abed El Rahman Hassoun − *GEOMAR Helmholtz Centre for Ocean Research Kiel, D-24105 Kiel, Germany; National Center for Marine Sciences, National Council for Scientific Research in Lebanon (CNRS-L), Beirut, Lebanon;* orcid.org/0000-0003-1940-215X

Fiz F. Pérez − *Instituto de Investigacións Mariñas (IIM), CSIC, DC 36208 Vigo, Spain*

Regina A. Easley − *Chemical Sciences Division, National Institute of Standards and Technology (NIST), DC 20899 Gaithersburg, Maryland, United States*

Marta Álvarez − *Centro Oceanográfico de A Coruña (COAC-IEO), CSIC, DC 15001 A Coruña, Spain;* orcid.org/0000-0002-5075-9344

Complete contact information is available at: https://pubs.acs.org/10.1021/acs.est.1c06083

Author Contributions

□E.F.G. and M.A. contributed equally to this work. All authors contributed to the interpretation of the data and the discussion of the results presented in the manuscript. All authors have given approval to the final version of the manuscript.

Funding

E.F.G. was supported by a Personal Técnico de Apoyo contract (PTA2016-12441-I) and N.M.F. was supported by a Juan de la Cierva postdoctoral contract (FJCI2015-24394), both from the Spanish Ministry of Science, Innovation and Universities and GAIN Grupo de Referencia Competitiva IN607A 2018/2 from Xunta de Galicia. M.I.G.-I. was supported by NOAA's Ocean Acidification Program (OAP) via Award No. NA17OAR0170332, and by NERC's CUSTARD (Carbon Uptake and Seasonal Traits of Antarctic Remineralisation Depths) project NE/P021263/1. A.E.R.H. was supported via the 2018 NF-POGO Shipboard Fellowship. F.F.P. was supported by the BOCATS2 (PID2019-104279GB-C21/AEI/10.13039/501100011033) project funded by MCIN/AEI/10.13039/501100011033 and contributing to WATER:iOS CSIC PTI. M.A. was supported by IEO RADIALES, RADPROF, and MEDSHIP18 programs. The MEDWAVES cruise was funded under the ATLAS project (Grant Agreement No. 678760). The RADPROF (2020) cruise was funded under the INTERREG Atlantic Area iFADO project. Useful and related discussions were held at the Ocean Carbonate System Intercomparison Forum working group funded by the Ocean Carbon Biogeochemistry program.

Notes

The authors declare no competing financial interest.

■ ACKNOWLEDGMENTS

This work was possible thanks to the commitment of agencies, principal investigators, scientists, technicians, and crew members acquiring high-quality hydrographic and biogeochemical data on transoceanic cruises and making them publicly available. The authors would like to thank Dr. Michael R. Winchester, Dr. Paul C. De Rose, and Dr. Jason F. Waters (NIST Materials Measurement Laboratory) for their helpful reviews. Certain commercial equipment, instruments, or materials are identified in this paper to specify the experimental procedure adequately. Such identification is not intended to imply recommendation or endorsement by NIST, nor is it intended to imply that the materials or equipment identified are necessarily the best available for the purpose. We are grateful for the comments of Dr. Andrew Dickson, Dr. Simone Alin, and a third anonymous reviewer.

■ ABBREVIATIONS

BK800	Beckman DU800 spectrophotometer
BY08	approach for measuring $[CO_3^{2-}]_{spec}$ described by Byrne and Yao[24]
CO_2	carbon dioxide
$[CO_3^{2-}]_{calc}$	calculated carbonate ion content from pH-TA or DIC-TA pairs
$[CO_3^{2-}]_{spec}$	spectrophotometric carbonate ion content
DIC	dissolved inorganic carbon
EAS13	approach for measuring $[CO_3^{2-}]_{spec}$ described by Easley et al.[28]
GOA-ON	Global Ocean Acidification Observing Network
OA	ocean acidification
PAT15	approach for measuring $[CO_3^{2-}]_{spec}$ described by Patsavas et al.[29]
PE850	PerkinElmer Lambda 850 spectrophotometer
R	absorbance ratio
SHA17	approach for measuring $[CO_3^{2-}]_{spec}$ described by Sharp et al.[30]
SHA19	approach for measuring $[CO_3^{2-}]_{spec}$ described by Sharp and Byrne[25]
SHI2401	Shimadzu UV2401 spectrophotometer
SHI2600	Shimadzu UV2600 spectrophotometer
TA	Total alkalinity

■ REFERENCES

(1) Friedlingstein, P.; Jones, M. W.; O'Sullivan, M.; Andrew, R. M.; Bakker, D. C. E.; Hauck, J.; Le Quéré, C.; Peters, G. P.; Peters, W.; Pongratz, J.; Sitch, S.; Canadell, J. G.; Ciais, P.; Jackson, R. B.; Alin, S. R.; Anthoni, P.; Bates, N. R.; Becker, M.; Bellouin, N.; Bopp, L.; Chau, T. T. T.; Chevallier, F.; Chini, L. P.; Cronin, M.; Currie, K. I.; Decharme, B.; Djeutchouang, L.; Dou, X.; Evans, W.; Feely, R. A.; Feng, L.; Gasser, T.; Gilfillan, D.; Gkritzalis, T.; Grassi, G.; Gregor, L.; Gruber, N.; Gürses, Ö.; Harris, I.; Houghton, R. A.; Hurtt, G. C.; Iida, Y.; Ilyina, T.; Luijkx, I. T.; Jain, A. K.; Jones, S. D.; Kato, E.; Kennedy, D.; Klein Goldewijk, K.; Knauer, J.; Korsbakken, J. I.; Körtzinger, A.; Landschützer, P.; Lauvset, S. K.; Lefèvre, N.; Lienert, S.; Liu, J.; Marland, G.; McGuire, P. C.; Melton, J. R.; Munro, D. R.; Nabel, J. E. M. S.; Nakaoka, S.-I.; Niwa, Y.; Ono, T.; Pierrot, D.; Poulter, B.; Rehder, G.; Resplandy, L.; Robertson, E.; Rödenbeck, C.; Rosan, T. M.; Schwinger, J.; Schwingshackl, C.; Séférian, R.; Sutton, A. J.; Sweeney, C.; Tanhua, T.; Tans, P. P.; Tian, H.; Tilbrook, B.; Tubiello, F.; van der Werf, G.; Vuichard, N.; Wada, C.; Wanninkhof, R.; Watson, A.; Willis, D.; Wiltshire, A. J.; Yuan, W.; Yue, C.; Yue, X.; Zaehle, S.; Zeng, J. Global Carbon Budget 2021. *Earth Syst. Sci. Data Discuss.* **2021**, *2021*, 1−191.

(2) Doney, S. C.; Fabry, V. J.; Feely, R. A.; Kleypas, J. A. Ocean Acidification: The Other CO_2 Problem. *Annu. Rev. Marine Sci.* **2009**, *1*, 169−192.

(3) Sabine, C. L.; Feely, R. A.; Gruber, N.; Key, R. M.; Lee, K.; Bullister, J. L.; Wanninkhof, R.; Wong, C. S.; Wallace, D. W. R.; Tilbrook, B.; Millero, F. J.; Peng, T.-H.; Kozyr, A.; Ono, T.; Rios, A. F. The Oceanic Sink for Anthropogenic CO_2. *Science* **2004**, *305* (5682), 367−371.

(4) Manabe, S.; Stouffer, R. J. Role of Ocean in Global Warming. *Journal of the Meteorological Society of Japan. Ser. II* **2007**, *85B*, 385−403.

(5) Xie, S.-P. Ocean Warming Pattern Effect On Global And Regional Climate Change. *AGU Advances* **2020**, *1* (1), e2019AV000130.

(6) Long, S.-M.; Xie, S.-P.; Du, Y.; Liu, Q.; Zheng, X.-T.; Huang, G.; Hu, K.-M.; Ying, J. Effects of Ocean Slow Response under Low Warming Targets. *Journal of Climate* **2020**, *33* (2), 477−496.

(7) Carstensen, J.; Duarte, C. M. Drivers of pH Variability in Coastal Ecosystems. *Environ. Sci. Technol.* **2019**, *53* (8), 4020−4029.

(8) Bates, N.; Astor, Y.; Church, M.; Currie, K.; Dore, J.; Gonaalez-Davila, M.; Lorenzoni, L.; Muller-Karger, F.; Olafsson, J.; Santa-Casiano, M. A Time-Series View of Changing Surface Ocean Chemistry Due to Ocean Uptake of Anthropogenic CO_2 and Ocean Acidification. *Oceanography* **2014**, *27* (1), 126−141.

(9) Talley, L. D.; Feely, R. A.; Sloyan, B. M.; Wanninkhof, R.; Baringer, M. O.; Bullister, J. L.; Carlson, C. A.; Doney, S. C.; Fine, R. A.; Firing, E.; Gruber, N.; Hansell, D. A.; Ishii, M.; Johnson, G. C.; Katsumata, K.; Key, R. M.; Kramp, M.; Langdon, C.; Macdonald, A. M.; Mathis, J. T.; McDonagh, E. L.; Mecking, S.; Millero, F. J.; Mordy, C. W.; Nakano, T.; Sabine, C. L.; Smethie, W. M.; Swift, J. H.; Tanhua, T.; Thurnherr, A. M.; Warner, M. J.; Zhang, J.-Z. Changes in Ocean Heat, Carbon Content, and Ventilation: A Review of the First Decade of GO-SHIP Global Repeat Hydrography. *Annu. Rev. Mar. Sci.* **2016**, *8* (1), 185−215.

(10) Hopkins, F. E.; Suntharalingam, P.; Gehlen, M.; Andrews, O.; Archer, S. D.; Bopp, L.; Buitenhuis, E.; Dadou, I.; Duce, R.; Goris, N.; Jickells, T.; Johnson, M.; Keng, F.; Law, C. S.; Lee, K.; Liss, P. S.; Lizotte, M.; Malin, G.; Murrell, J. C.; Naik, H.; Rees, A. P.; Schwinger, J.; Williamson, P. The Impacts of Ocean Acidification on Marine Trace Gases and the Implications for Atmospheric Chemistry and Climate. *Proc. R. Soc. A* **2020**, *476* (2237), 20190769.

(11) Feely, R. A.; Doney, S. C.; Cooley, S. R. Ocean Acidification. *Oceanography* **2009**, *22* (4), 36−47.

(12) Andersson, A. J.; Kline, D. I.; Edmunds, P. J.; Archer, S. D.; Bednaršek, N.; Carpenter, R. C.; Chadsey, M.; Goldstein, P.; Grottoli, A. G.; Hurst, T. P.; King, A. L.; Kübler, J. E.; Kuffner, I. B.; Mackey, K. R. M.; Menge, B. A.; Paytan, A.; Riebesell, U.; Schnetzer, A.; Warner, M. E.; Zimmerman, R. C. Understanding Ocean Acidification Impacts on Organismal to Ecological Scales. *Oceanography* **2015**, *25* (2), 16−27.

(13) Doney, S. C.; Busch, D. S.; Cooley, S. R.; Kroeker, K. J. The Impacts of Ocean Acidification on Marine Ecosystems and Reliant Human Communities. *Annu. Rev. Environ. Resour.* **2020**, *45* (1), 83−112.

(14) Bach, L. T.; Riebesell, U.; Gutowska, M. A.; Federwisch, L.; Schulz, K. G. A Unifying Concept of Coccolithophore Sensitivity to Changing Carbonate Chemistry Embedded in an Ecological Framework. *Progress in Oceanography* **2015**, *135*, 125−138.

(15) Feely, R. A.; Sabine, C. L.; Lee, K.; Berelson, W.; Kleypas, J.; Fabry, V. J.; Millero, F. J. Impact of Anthropogenic CO_2 on the $CaCO_3$ System in the Oceans. *Science* **2004**, *305* (5682), 362−366.

(16) Zeebe, R. E.; Wolf-Gladrow, D. *CO_2 in Seawater: Equilibrium, Kinetics, Isotopes*; Elsevier Science, 2001; Vol. *65*.

(17) Dickson, A. G., Sabine, C. L., Christian, J. R., Bargeron, C. P. *Guide to Best Practices for Ocean CO_2 Measurements*; PICES special publication; North Pacific Marine Science Organization: Sidney, BC, 2007.

(18) Riebesell, U.; Fabry, V.; Hansson, L.; Gatusso, J. P. *Guide to Best Practices for Ocean Acidification Research and Data Reporting*; Publications Office of the European Union: LU, 2011.

https://doi.org/10.1021/acs.est.1c06083
Environ. Sci. Technol. 2022, 56, 7381−7395

(19) Bushinsky, S. M.; Takeshita, Y.; Williams, N. L. Observing Changes in Ocean Carbonate Chemistry: Our Autonomous Future. *Current Climate Change Reports* **2019**, *5* (3), 207−220.
(20) Claustre, H.; Johnson, K. S.; Takeshita, Y. Observing the Global Ocean with Biogeochemical-Argo. *Annu. Rev. Mar. Sci.* **2020**, *12* (1), 23−48.
(21) Ma, J.; Shu, H.; Yang, B.; Byrne, R. H.; Yuan, D. Spectrophotometric Determination of pH and Carbonate Ion Concentrations in Seawater: Choices, Constraints and Consequences. *Anal. Chim. Acta* **2019**, *1081*, 18−31.
(22) Patsavas, M. C.; Byrne, R. H.; Wanninkhof, R.; Feely, R. A.; Cai, W.-J. Internal Consistency of Marine Carbonate System Measurements and Assessments of Aragonite Saturation State: Insights from Two U.S. Coastal Cruises. *Marine Chemistry* **2015**, *176*, 9−20.
(23) McLaughlin, K.; Weisberg, S.; Dickson, A.; Hofmann, G.; Newton, J.; Aseltine-Neilson, D.; Barton, A.; Cudd, S.; Feely, R.; Jefferds, I.; Jewett, E.; King, T.; Langdon, C.; McAfee, S.; Pleschner-Steele, D.; Steele, B. Core Principles of the California Current Acidification Network: Linking Chemistry, Physics, and Ecological Effects. *oceanog* **2015**, *25* (2), 160−169.
(24) Byrne, R. H.; Yao, W. Procedures for Measurement of Carbonate Ion Concentrations in Seawater by Direct Spectrophotometric Observations of Pb(II) Complexation. *Marine Chemistry* **2008**, *112* (1), 128−135.
(25) Sharp, J. D.; Byrne, R. H. Carbonate Ion Concentrations in Seawater: Spectrophotometric Determination at Ambient Temperatures and Evaluation of Propagated Calculation Uncertainties. *Marine Chemistry* **2019**, *209*, 70−80.
(26) Shangguan, Q.; Shu, H.; Li, P.; Lin, K.; Byrne, R. H.; Li, Q.; Yuan, D.; Ma, J. Automated Spectrophotometric Determination of Carbonate Ion Concentration in Seawater Using a Portable Syringe Pump Based Analyzer. *Marine Chemistry* **2019**, *209*, 120−127.
(27) Byrne, R. H. Inorganic Lead Complexation in Natural Seawater Determined by UV Spectroscopy. *Nature* **1981**, *290* (5806), 487−489.
(28) Easley, R. A.; Patsavas, M. C.; Byrne, R. H.; Liu, X.; Feely, R. A.; Mathis, J. T. Spectrophotometric Measurement of Calcium Carbonate Saturation States in Seawater. *Environ. Sci. Technol.* **2013**, *47* (3), 1468−1477.
(29) Patsavas, M. C.; Byrne, R. H.; Yang, B.; Easley, R. A.; Wanninkhof, R.; Liu, X. Procedures for Direct Spectrophotometric Determination of Carbonate Ion Concentrations: Measurements in US Gulf of Mexico and East Coast Waters. *Marine Chemistry* **2015**, *168*, 80−85.
(30) Sharp, J. D.; Byrne, R. H.; Liu, X.; Feely, R. A.; Cuyler, E. E.; Wanninkhof, R.; Alin, S. R. Spectrophotometric Determination of Carbonate Ion Concentrations: Elimination of Instrument-Dependent Offsets and Calculation of In Situ Saturation States. *Environ. Sci. Technol.* **2017**, *51* (16), 9127−9136.
(31) Soli, A. L.; Stewart, Z. I.; Byrne, R. H. The Influence of Temperature on $PbCO_3^0$ Formation in Seawater. *Marine Chemistry* **2008**, *110* (1), 1−6.
(32) Luo, Y.; Millero, F. J. Stability Constants for the Formation of Lead Chloride Complexes as a Function of Temperature and Ionic Strength. *Geochim. Cosmochim. Acta* **2007**, *71* (2), 326−334.
(33) Easley, R. A.; Byrne, R. H. The Ionic Strength Dependence of Lead (II) Carbonate Complexation in Perchlorate Media. *Geochim. Cosmochim. Acta* **2011**, *75* (19), 5638−5647.
(34) Clayton, T. D.; Byrne, R. H. Spectrophotometric Seawater pH Measurements: Total Hydrogen Ion Concentration Scale Calibration of m-Cresol Purple and at-Sea Results. *Deep Sea Research Part I: Oceanographic Research Papers* **1993**, *40* (10), 2115−2129.
(35) Álvarez, M.; Pérez, F. F.; Fernández Guallart, E.; Castaño, M.; Fajar, N. M.; García-Ibáñez, M. I.; Santiago-Domenech, R.; El Rahman Hassoun, A. Ten Years of Spanish Ion Carbonate Data in the North Atlantic Ocean and Mediterranean Sea. *Digital CSIC*, 2021. DOI: 10.20350/digitalCSIC/13786.
(36) Olsen, A.; Lange, N.; Key, R. M.; Tanhua, T.; Bittig, H. C.; Kozyr, A.; Álvarez, M.; Azetsu-Scott, K.; Becker, S.; Brown, P. J.; Carter, B. R.; Cotrim da Cunha, L.; Feely, R. A.; van Heuven, S.; Hoppema, M.; Ishii, M.; Jeansson, E.; Jutterström, S.; Landa, C. S.; Lauvset, S. K.; Michaelis, P.; Murata, A.; Pérez, F. F.; Pfeil, B.; Schirnick, C.; Steinfeldt, R.; Suzuki, T.; Tilbrook, B.; Velo, A.; Wanninkhof, R.; Woosley, R. J. An Updated Version of the Global Interior Ocean Biogeochemical Data Product, GLODAPv2.2020. *Earth System Science Data* **2020**, *12* (4), 3653−3678.
(37) Orr, J. C.; Epitalon, J.-M.; Dickson, A. G.; Gattuso, J.-P. Routine Uncertainty Propagation for the Marine Carbon Dioxide System. *Marine Chemistry* **2018**, *207*, 84−107.
(38) Álvarez, M.; Fajar, N. M.; Carter, B. R.; Guallart, E. F.; Pérez, F. F.; Woosley, R. J.; Murata, A. Global Ocean Spectrophotometric pH Assessment: Consistent Inconsistencies. *Environ. Sci. Technol.* **2020**, *54* (18), 10977−10988.
(39) Pérez, F. F.; Rios, A. F.; Rellán, T.; Alvarez, M. Improvements in a Fast Potentiometric Seawater Alkalinity Determination. *Ciencias Marinas* **2000**, *26* (3), 463−478.
(40) Pérez, F. F.; Fraga, F. A Precise and Rapid Analytical Procedure for Alkalinity Determination. *Marine Chemistry* **1987**, *21* (2), 169−182.
(41) Mintrop, L.; Pérez, F. F.; González Dávila, M.; Santana-Casiano, J. M.; Körtzinger, A. Alkalinity Determination by Potentiometry: Intercalibration Using Three Different Methods *Ciencias Marinas* **2000***26*, DOI: 10.7773/cm.v26i1.573
(42) Johnson, K. M.; Dickson, A. G.; Eischeid, G.; Goyet, C.; Guenther, P.; Key, R. M.; Millero, F. J.; Purkerson, D.; Sabine, C. L.; Schottle, R. G.; et al. Coulometric Total Carbon Dioxide Analysis for Marine Studies: Assessment of the Quality of Total Inorganic Carbon Measurements Made during the US Indian Ocean CO_2 Survey 1994−1996. *Marine Chemistry* **1998**, *63* (1−2), 21−37.
(43) Dickson, A. G.; Afghan, J. D.; Anderson, G. C. Reference Materials for Oceanic CO_2 Analysis: A Method for the Certification of Total Alkalinity. *Marine Chemistry* **2003**, *80* (2), 185−197.
(44) Fajar, N. M.; García-Ibáñez, M. I.; SanLeón-Bartolomé, H.; Álvarez, M.; Pérez, F. F. Spectrophotometric Measurements of the Carbonate Ion Concentration: Aragonite Saturation States in the Mediterranean Sea and Atlantic Ocean. *Environ. Sci. Technol.* **2015**, *49* (19), 11679−11687.
(45) Van Heuven, S.; Pierrot, D.; Rae, J. W. B.; Lewis, E.; Wallace, D. W. R. *MATLAB Program Developed for CO_2 System Calculations*; ORNL/CDIAC-105b, 2011; p *530*.
(46) Mehrbach, C.; Culberson, C. H.; Hawley, J. E.; Pytkowicx, R. M. Measurement of the Apparent Dissociation Constants of Carbonic Acid in Seawater at Atmospheric Pressure. *Limnology and Oceanography* **1973**, *18* (6), 897−907.
(47) Lueker, T. J.; Dickson, A. G.; Keeling, C. D. Ocean pCO_2 Calculated from Dissolved Inorganic Carbon, Alkalinity, and Equations for K_1 and K_2: Validation Based on Laboratory Measurements of CO_2 in Gas and Seawater at Equilibrium. *Marine Chemistry* **2000**, *70* (1), 105−119.
(48) Dickson, A. G. Standard Potential of the Reaction: $AgCl(s) + 12H_2(g) = Ag(s) + HCl(Aq)$, and and the Standard Acidity Constant of the Ion HSO_4^- in Synthetic Sea Water from 273.15 to 318.15 K. *J. Chem. Thermodyn.* **1990**, *22* (2), 113−127.
(49) Lee, K.; Kim, T.-W.; Byrne, R. H.; Millero, F. J.; Feely, R. A.; Liu, Y.-M. The Universal Ratio of Boron to Chlorinity for the North Pacific and North Atlantic Oceans. *Geochim. Cosmochim. Acta* **2010**, *74* (6), 1801−1811.
(50) Newton, J.; Feely, R.; Jewett, E.; Williamson, P.; Mathis, J. *Global Ocean Acidification Observing Network: Requirements and Governance Plan*, 2nd ed.; GOA-ON, 2015, http://www.goa-on.org/docs/GOA-ON_plan_print.pdf; p 61.
(51) Fong, M. B.; Dickson, A. G. Insights from GO-SHIP Hydrography Data into the Thermodynamic Consistency of CO_2 System Measurements in Seawater. *Marine Chemistry* **2019**, *211*, 52−63.

SUPPORTING INFORMATION for:

Spectrophotometric measurement of carbonate ion in seawater along a decade: dealing with inconsistencies

Elisa F. Guallart[*,1,2], Noelia M. Fajar[1,3], Maribel I. García-Ibáñez[4,2], Mónica Castaño-Carrera[1], Rocío Santiago-Doménech[5], Abed El Rahman Hassoun[6,7], Fiz F. Pérez[3], Regina A. Easley[8], Marta Álvarez[1]

[1] Centro Oceanográfico de A Coruña (COAC-IEO), CSIC, DC 15001 A Coruña, Spain

[2] Institut de Ciències del Mar (ICM), CSIC, DC 08003 Barcelona, Spain

[3] Instituto de Investigacións Mariñas (IIM), CSIC, DC 36208 Vigo, Spain

[4] School of Environmental Sciences, University of East Anglia (UEA), Norwich NR47TJ, United Kingdom

[5] Centro Oceanográfico de Baleares (COB-IEO), CSIC, DC 07015 Palma de Mallorca, Balearic Islands, Spain

[6] GEOMAR Helmholtz Centre for Ocean Research Kiel, D- 24105 Kiel, Germany

[7] National Center for Marine Sciences, National Council for Scientific Research in Lebanon (CNRS-L), Beirut, Lebanon.

[8] Chemical Sciences Division, National Institute of Standards and Technology (NIST), MS 8391, Gaithersburg, MD 20899, United States

Corresponding author:

**e-mail: efguallart@icm.csic.es*; phone (+34) 932309500; fax: (+34)932309555.

Number of pages: 24

Number of figures: 7

Number of tables: 5

Appendix A: Global ocean distribution of carbonate ion content and saturation states.

The saturation state (Ω) of calcium carbonate ($CaCO_3$) minerals is defined as:

$$\Omega = [Ca^{2+}] [CO_3^{2-}] / K_{sp} \quad (S1)$$

where $[CO_3^{2-}]$ is the carbonate ion content, $[Ca^{2+}]$ is the calcium content, and K_{sp} is the apparent stoichiometric solubility product for a given $CaCO_3$ mineral phase, calcite or aragonite. The solubility of both compounds increases slightly at lower temperature and strongly with increasing pressure. Since $[Ca^{2+}]$ is closely proportional to salinity, Ω is largely determined by in situ $[CO_3^{2-}]$ variations with regard to in situ $[CO_3^{2-}]$ saturation. The depth at which $CaCO_3$ minerals, aragonite and calcite, are in equilibrium is known as the saturation depth or saturation horizon (Ω = 1). There is a pronounced shoaling of the saturation horizons of both minerals from the Atlantic to the Indian and then to the Pacific oceans. This occurs because of the lower total alkalinity (TA) to dissolved inorganic carbon (DIC) ratio (TA/DIC) in the intermediate and deep waters of the latter two oceans relative to the Atlantic. Among oceans, the aragonite saturation horizon is always shallower than the calcite saturation horizon due to its higher solubility.[1,2]

In the surface ocean, warmer and saltier regions show higher $[CO_3^{2-}]$ and are more saturated with respect to $CaCO_3$ minerals than colder and less saline regions (Figure S1A and B). Evaporation (precipitation) processes that increase (decrease) salinity levels cause a TA and DIC increase (reduction) in a 2:1 ratio.[3] High TA/DIC waters with a higher buffer capacity present, accordingly, high values of $[CO_3^{2-}]$ and Ω for aragonite, $\Omega_{aragonite}$ (Figure S1A and B). In addition, the buffer factor ($-\omega_{DIC}$; in $mmol \cdot kg^{-1}$)[4] showing the fractional change in $\Omega_{aragonite}$ for changes in DIC when TA is constant, decreases as the TA/DIC ratio increases (Figure S1C). Therefore, for a given increase in DIC due to anthropogenic carbon uptake, the decrease in Ω is higher for high TA/DIC waters.

The lower row panels in Figure S1 show the same variables as the upper panels: in situ $[CO_3^{2-}]$, $\Omega_{aragonite}$, and $-\omega_{DIC}$ for the full-depth merged dataset reported in this study, evidencing the broad range of oceanic conditions covered with regard to the global ocean ranges.

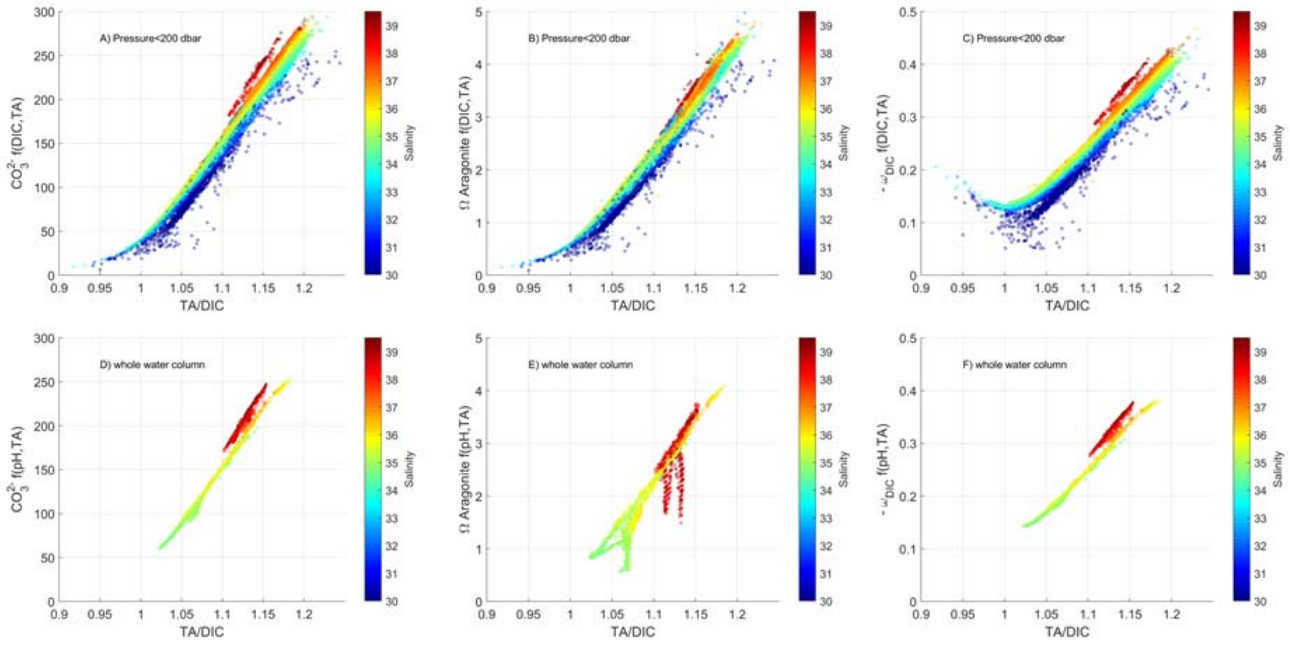

Figure S1. Distribution of (A and D) in situ [CO_3^{2-}] (CO_3^{2-}; in µmol·kg^{-1}), (B and E) in situ aragonite saturation ($\Omega_{aragonite}$; dimensionless), and (C and F) in situ buffer factor ($-\omega_{DIC}$; in mmol·kg^{-1}) as a function of the TA to DIC ratio (TA/DIC). Upper panels show calculated variables from the global surface ocean (pressure < 200 dbar) DIC and TA data from GLODAPv2.2019.[5] Lower panels show the calculated variables from full water column pH and TA from the merged dataset in this study (Table 1). See Section 2.2 regarding thermodynamic CO_2 calculations. The z-axis shows salinity in color scale**.**

Appendix B: Evolution of the methodology for measuring carbonate ion content.

The formation of lead carbonate ($PbCO_3^0$) in seawater is given by:

$$Pb^{2+} + CO_3^{2-} \leftrightarrow PbCO_3^0 \quad (S2)$$

The formation (or stability) constant for $PbCO_3^0$, ${}_{CO3}\beta_1$, refers to the equilibrium constant for the formation of $PbCO_3^0$ in solution and is a measure of the strength of the interaction between $[Pb^{2+}]_T$ and $[CO_3^{2-}]_T$ to form $PbCO_3^0$. It is given by:

$${}_{CO3}\beta_1 = \frac{[PbCO_3^0]}{[Pb^{2+}]_T[CO_3^{2-}]_T} \quad (S3)$$

where $[Pb^{2+}]_T$ represents the total amount of content of free Pb^{2+}, Pb(II)-chloride species and minor amounts of Pb(II)-sulfate species. $[CO_3^{2-}]_T$ is the total amount of content of free and ion-paired carbonate and $[PbCO_3^0]$ represents the total amount of content of Pb(II) complexed with carbonate, including contributions from mixed ligand species. All amounts of substance content are given in $\mu mol \cdot kg^{-1}$ of seawater.

When Pb(II) complexes with $[CO_3^{2-}]_T$ in Pb(II)-enriched seawater, the ultraviolet spectrum of the solution is affected and $[CO_3^{2-}]_T$ can be determined spectrophotometrically ($[CO_3^{2-}]_{spec}$) through Equation (1) in the main manuscript. This equation allows for the direct determination of $[CO_3^{2-}]_{spec}$ in terms of the ratio of Pb(II) absorbances of the sample at two given wavelengths (R value; Equation (2)), provided that the remaining terms in Equation (1) ($\log\{{}_{CO3}\beta_1/e_2\}$, e_1, and e_3/e_2) have been accurately characterized.

Table S1 summarizes the main features of the five different approaches that have been described for the determination of $[CO_3^{2-}]_{spec}$ since 2008, as the methodology has been periodically revised, here abbreviated as BY08,[6] EAS13,[7] PAT15,[8] SHA17,[9] and SHA19.[10] Table S1 reports the different conditions at which the terms $\log\{{}_{CO3}\beta_1/e_2\}$, e_1, and e_3/e_2 in Equation (1) were characterized for each approach. In fact, the characterization of these terms is implicitly a calibration because it relates a given R value to a particular $[CO_3^{2-}]_T$ and, thus, the existence of various sets of calibration functions, one per approach, that yield five different $[CO_3^{2-}]_{spec}$ values from a single R measurement, is in practice equivalent to having five different methods for measuring $[CO_3^{2-}]_{spec}$. In this regard, the five approaches overall followed the same fitting procedure for calibrating the spectrophotometric terms in Equation (1) that consists of making R measurements in seawater over a range of conditions (e.g., salinity and temperature) where the seawater has been independently analyzed for at least two of the usually measured CO_2 system parameters (e.g., pH, TA, and DIC). It is then possible to calculate a value for $[CO_3^{2-}]_T$ ($[CO_3^{2-}]_{calc}$) from the application of a given equilibrium model for seawater, taking account of all acid-base systems occurring in the sample, and seeking to fit the terms $\log\{{}_{CO3}\beta_1/e_2\}$, e_1, and e_3/e_2 as

functions of salinity and temperature. Table S2 summarizes the reported calibration functions for $\log\{_{CO3}\beta_1/e_2\}$, e_1, and e_3/e_2 in Equation (1) for each of the five approaches as a function of salinity (BY08, EAS13, PAT15, and SHA17; all values referred to 25 ºC) and also temperature (SHA19). All formulations are referred to atmospheric pressure.

The successive reformulations of the calibration functions (Table S2) have, in turn, been fostered by successive reviews and upgrades of the methodological procedure proposed to obtain accurate enough values of *R*. Note that any change in the procedure to determine *R* implicitly forces the reformulation of the calibration equations that relate *R* values with given amounts of $[CO_3^{2-}]_{calc}$. In this regard, *R* values are affected by (Table 1): i) the Pb(II) reagent, ii) the spectrophotometer used, and iii) additional corrections to readjust measured *R* values into "closer to the true" values (Equations (4) and (5)). On the other hand, the $[CO_3^{2-}]_{calc}$ data used can also impact the fitting of the calibration functions, through (Table 1): i) the thermodynamic model of seawater assumed (i.e., CO_2 system constants and the other constants of known acid-base systems), ii) the quality of the measurements of the two CO_2 systems parameters used as input for obtaining $[CO_3^{2-}]_{calc}$ (pH, TA, and DIC) and iii) the ranges of $[CO_3^{2-}]$ studied (i.e., the region of study and the use of natural versus laboratory-modified seawater).

BY08 characterized the first set of calibration functions for the terms $\log\{_{CO3}\beta_1/e_2\}$, e_1, and e_3/e_2 in Equation (1) (Table S2). They constrained the corresponding terms experimentally in seawater modified in the laboratory and characterized the Pb(II) absorbance response (*R* values; Equation (2)) by using lead chloride ($PbCl_2$) (Table S1).

EAS13 reviewed the approach of BY08 using natural seawater samples and pH values measured spectrophotometrically with purified dye (Table 1). EAS13 found significant biases in the $[CO_3^{2-}]$ residuals (observations with respect to calculated values) obtained with their approach at $[CO_3^{2-}]_{calc} \geq 150$ μmol·kg^{-1}, evidencing the underestimation of $[CO_3^{2-}]_{spec}$ measurements at higher amounts of content. EAS13 related those results to a possible lack of applicability of the Pb(II) complexation model (Equation S2) at high pH values,[11] suggesting that it should likely be extended to the formation of the $Pb(CO_3)_2^{2-}$ species.

The review of the methodology reported by PAT15 proposed a change in the reagent used for characterizing the *R* values, using lead perchlorate ($Pb(ClO_4)_2$) instead of $PbCl_2$ to increase the signal-to-noise ratio of the absorbance measurements. This change also doubled the final Pb(II) concentration in the cuvette with regard to former protocols (Table S1). Consequently, PAT15 proposed an additional correction for readjusting the measured *R* data (Equation (4)) because of the perturbation of the sample due to the Pb(II) reagent addition. PAT15 refitted the calibration functions (Table S2) according to new field data, with the overall aim of improving the determination of $[CO_3^{2-}]_{spec}$ well above 180 μmol·kg^{-1}. PAT15 did assume another

thermodynamic model for $[CO_3^{2-}]_{calc}$ with regard to BY08 and EAS13 (Table S1). The authors kept using the e_3/e_2 term described by BY08 and proposed new values for $\log\{_{CO3}\beta_1/e_2\}$ and e_1 (Table S2). The approach by PAT15 yielded $[CO_3^{2-}]_{spec}$ that were accurate enough over a large range of amount of carbonate content (about 75 $\mu mol \cdot kg^{-1}$ – 260 $\mu mol \cdot kg^{-1}$) but the authors stated that further work would be required to assess the applicability of the new Pb(II) reagent and the refitted calibration functions for low-carbonate (i.e., at lower salinity) waters. PAT15 attributed the observed residuals between observations and calculated values to the underlying chemical measurements of the input parameters for estimating $[CO_3^{2-}]_{calc}$, not to differences in the fitting protocols for characterizing the calibration functions, nor to the potential lack of applicability of the Pb(II) complexation model at high pH values.[11]

The reviews by EAS13 and PAT15 aimed mainly to improve the parametrization of the complexation between $[Pb^{2+}]_T$ and $[CO_3^{2-}]_T$ by refitting the calibration functions of the terms in Equation (1) into values representative of natural seawater by enlarging the range of ocean conditions, mainly salinity, assessed to fit them (Table S1). The following review of the methodology by SHA17 deviates from this rationale and suggests that carbonate residuals between observations and calculated values are mainly attributable to the spectrophotometer equipment through potential calibration offsets of the particular spectrophotometer used for measuring the absorbances needed for obtaining the *R* data. Uncalibrated equipment might produce artifacts in the UV signal at the measured wavelengths, generating incongruent *R* and $[CO_3^{2-}]_{spec}$ values. The authors also used $Pb(ClO_4)_2$ for measuring *R*. In SHA17, no perturbation correction (Equation (4)) was recommended. Instead, they reported an equation for correcting measured *R* as a function of a wavelength offset term (Equation (5)) (Table 1). SHA17 also recharacterized the calibration functions (Table S2). Additionally, the authors recommended recording Pb(II) absorbances at wavelengths surrounding the primary target wavelengths (e.g., 233 nm, 234 nm, and 235 nm) because of the use of multi-wavelength measurement techniques in the future.

Finally, SHA19 reported the most recent review of the calibration functions. The authors did not change the procedure to obtain R^0 with regard to SHA17(Table S2) but extended the characterization of the terms over a broader range of salinity and temperature to enable in situ observations by combining field datasets from former works with laboratory data (Table S1).

Table S1. Summary of fitting conditions for the characterization of the terms $\log\{_{CO3}\beta_1/e_2\}$, e_1, and e_3/e_2 in Equation (1) for the five approaches of the spectrophotometric technique to measure carbonate ion in seawater abbreviated as BY08,[6] EAS13,[7] PAT15,[8] SHA17,[9] and SHA19[10]. SW stands for seawater. $pH_{electrode}$ stands for seawater pH measured with an electrode calibrated on the total scale in natural seawater whose pH was determined with thymol blue dye, and pH_{pur} stands for seawater pH on the total scale measured with purified m-cresol dye. DIC stands for dissolved inorganic carbon, and TA for total alkalinity, both in $\mu mol \cdot kg^{-1}$. *S* stands for salinity, *t* for temperature in ºC, $[CO_3^{2-}]_{calc}$ is the amount of carbonate ion content calculated from paired measured CO_2 variables, K_1 and K_2 stand for the first and second CO_2 equilibrium constants, K_{HSO4} for the bisulfate constant, K_B for the boric acid constant and TB for the total boron-to-chlorinity ratio. *R* corresponds to de absorbance ratio of Pb(II) at two wavelengths (Equation (2)). R^0 corresponds to the initial ratio before perturbation of the sample due to Pb(II) reagent addition for PAT15 (Equation (4)), and to the ratio corrected for wavelength offsets of the spectrophotometer for SHA17 and SHA19. $\Delta\lambda_{241.1}$ is the spectrophotometer-specific wavelength offset at λ = 241.10 nm, defined as the wavelength location of a holmium oxide standard absorbance peak as specified by the manufacturer minus the wavelength at which the spectrophotometer reports the peak, which causes a reversal in the sign of Equation (5) with regard to SHA17. The $[CO_3^{2-}]_{spec}$ precision (in $\mu mol \cdot kg^{-1}$ or %) and the $[CO_3^{2-}]_{spec}$ standard uncertainty (in %) are reported for each method approach.

Table S1	BY08	EAS13	PAT15	SHA17	SHA19
Pb(II) reagent	$PbCl_2$	$PbCl_2$	$Pb(ClO_4)_2$	$Pb(ClO_4)_2$	$Pb(ClO_4)_2$
[Pb(II); µmol·L^{-1}] in 10cm pathlength cuvette	7.5	7.5	15.2	15.2	15.2
Region of study	-	US West Coast and Arctic	US East Coast and Gulf of Mexico	US East and West coasts	As in PAT15 and SHA17
Laboratory data	yes (modified Gulf of Mexico SW)	no	no	no	yes (modified Gulf of Mexico SW)
Measured CO_2 system variables	$pH_{electrode}$, TA	pH_{pur}, DIC, TA	pH_{pur}, DIC, TA	pH_{pur}, DIC	pH_{pur}, DIC, TA
$[CO_3^{2-}]_{calc}$ range in µmol·kg^{-1}	$68<[CO_3^{2-}]_{calc}<400$	$38<[CO_3^{2-}]_{calc}<258$	$73<[CO_3^{2-}]_{calc}<258$	$68<[CO_3^{2-}]_{calc}<258$	As in PAT15 and SHA17
***S* range**	20<S<36	26.6<S<34.9	28.6<S<36.6	34.50<S<36.72	20<S<40
CO_2 system and other constants used for $[CO_3^{2-}]_{calc}$	K_1&K_2 Mehrbach et al.[12] as refit by Dickson and Millero;[13] K_{HSO4}, K_B and TB not reported	K_1&K_2 Mehrbach et al. [12] as refit by Dickson and Millero;[13] K_{HSO4} Dickson,[14a] K_B Dickson,[15a] TB not reported	K_1&K_2 Lueker et al.,[16] K_{HSO4} Dickson,[14] TB Lee et al. [17]	As in PAT15	As in PAT15
***t* range**	25 ºC ± 0.05 ºC	25 ºC ± 0.05 ºC	25 ºC ± 0.05 ºC	25 ºC ± 0.05 ºC	3 ºC < *t* ± 0.05 ºC < 40 ºC
Spectrophotometer	HP Agilent 8453	HP Agilent 8453	HP Agilent 8453	HP Agilent 8453	HP Agilent 8453
Pb(II) reagent addition correction	not evaluated	evaluated, no correction applied	evaluated, correction applied $\log(R\text{-}R^0)=$ $-17.6664R^2+19.8995R-7.7324$	evaluated, no correction applied	evaluated, no correction applied
Wavelength offset correction	not identified	not identified	not identified	identified $R^0 = R + 0.0265 \times \Delta\lambda_{241.1}$	As in SHA17
$[CO_3^{2-}]_{spec}$ precision, in µmol·kg^{-1} or %	not reported	± 1.7, ± 2.28 %	not reported	± 1.9 µmol·kg^{-1}	± 0.7 %
$[CO_3^{2-}]_{spec}$ standard uncertainty in %	± 2% or less	± 2.3 %	± 2.1 %	± 1.5 %	± 2 %

[a] K_{HSO4} and KB in EAS13 added as R. Easley personal communication

Table S2. Summary of the coefficients for the spectrophotometric terms in Equation (1) to calculate $[CO_3^{2-}]_{spec}$ in seawater according to the five different approaches (Table S1). Each parameter is expressed with the general equation form of *Z*, following Sharp and Byrne.[10] The different approaches are denoted as BY08,[6] EAS13,[7] PAT15,[8] SHA17,[9] and SHA19.[10] *S* is salinity and *t* is temperature in ºC. Formulations by BY08, EAS13, PAT15, and SHA17 are referred to 25 ºC, being only salinity-dependent. The approach by SHA19 is also temperature-dependent (Table S1). All coefficients apply to a pressure of 1 atm.

$$Z = a_0 + b_0 S + b_1 S^2 + C_0 t + C_1 t^2 + d_0 S t$$

Z		$a_0 \cdot 10$	$b_0 \cdot 10^3$	$b_1 \cdot 10^4$	$c_0 \cdot 10^3$	$c_1 \cdot 10^5$	$d_0 \cdot 10^5$
	BY08	60.87	-84.95	9.36	-	-	-
	EAS13	55.13	-53.58	5.166	-	-	-
log(β/e₂)	PAT15	55.07074	-41.259	1.8	-	-	-
	SHA17	68.7057	-142.142	19.0892	-	-	-
	SHA19	55.6674	-51.0194	4.61423	-	-	-13.6998
	BY08	2.215	-0.5554	0.844	-	-	-
	EAS13	2.293	-0.5554	0.844	-	-	-
e1	PAT15	3.11907	-2.396	0.8	-	-	-
	SHA17	7.87458	-33.9648	5.83574	-	-	-
	SHA19	1.09519	4.49666	-	1.95519	2.4446	-2.01796
	BY08	30.61	-87.3	9.363	-	-	-
	EAS13	30.91	-87.3	9.363	-	-	-
e3/e2	PAT15	30.61	-87.3	9.363	-	-	-
	SHA17	25.2288	-38.3205	-	-	-	-
	SHA19	32.4812	-79.7676	6.28521	-11.8691	-3.58709	32.5849

The calibration functions that describe $\log\{_{CO3}\beta_1/e_2\}$, e_1, and e_3/e_2) in Equation (1) seem to have come up with differing values for them (Table S2). To better compare the effect of the differing values for these terms on $[CO_3^{2-}]_{spec}$, Equation (1) in the main manuscript can be algebraically transformed to express $[CO_3^{2-}]_{spec}$ in µmol·kg^{-1} as follows:

$$[CO_3^{2-}]_{spec} = \left[10^6 * 10^{\log\left[\frac{CO3\beta_1}{e_2}\right]}\right] * \left[\frac{1}{R - e_1}\right] * \left[1 - R * \frac{e_3}{e_2}\right] \quad (S4)$$

Figures S2 and S3 show the terms between brackets in Equation (S4) for the different approaches. The inset in Figure S2A shows $[CO_3^{2-}]_{spec}$ at 25 ºC and salinity 35 as a function of *R*, which clearly increase as *R* decreases. For the same conditions in temperature and salinity, $[CO_3^{2-}]_{spec}$ as a function of *R* by EAS13 is about 5 % higher than by BY08 at $[CO_3^{2-}]_{spec}$ > 150 µmol.kg^{-1} or *R* < 0.46, and about 5 % lower for higher *R* values (Figure S2A). PAT15, SHA17, and SHA19 approaches return $[CO_3^{2-}]_{spec}$ values higher than BY08 for the whole *R* range, being larger than 10 % for $[CO_3^{2-}]_{spec}$ > 150 µmol·kg^{-1} (*R* < 0.46), particularly with the PAT15 approach (Figure S2A).

The first term in Equation (S4), $\left[10^6 * 10^{\log\left[\frac{CO3\beta_1}{e_2}\right]}\right]$ (in µmol·kg^{-1}), is only marginally dependent on temperature when using SHA19 formulations, being mostly dependent on salinity for all the approaches (Table S2) and increases with it (inset in Figure S2B). This is directly linked to the presence of more carbonate ion content in higher salinity waters (Figure S1). This first term in Equation (S4) is similar for BY08 and EAS13, with EAS13 being slightly lower (Figure S2B). However, in PAT15, SHA17, and SHA19 the relation with salinity differs with regard to BY08 and also between them across the salinity range. Results among approaches are close between them at about ± 5 % only at salinity around 37 ± 1, except for SHA19.

This first term in Equation (S4) $\left[10^6 * 10^{\log\left[\frac{CO3\beta_1}{e_2}\right]}\right]$ is modulated upwards by $\left[\frac{1}{R-e_1}\right]$ and downwards by $\left[1 - R * \frac{e_3}{e_2}\right]$ (Figure S3). Regarding these two terms, the main changes in the evolution of the methodology relate to the $\left[\frac{1}{R-e_1}\right]$ term (upper row in Figure S3), which is related to higher carbonate ion content (lower *R* values), where more remarkable inconsistencies between spectrophotometric and calculated carbonate ion content have been found.[7–10,18] In this regard, the greatest changes were introduced by PAT15 and SHA19 (Figure S3C and S3E) in low salinity waters, while SHA17 introduced the changes for high salinity waters (Figure S3D). The term $\left[1 - R \cdot \frac{e_3}{e_2}\right]$ most strongly influences carbonate ion calculations at low carbonate content (Figure S3F-J) and has slightly changed with regard to BY08 overall. PAT15 reported the same coefficients for this term, being SHA17 and SHA19 who introduced the greatest modifications compared to BY08.

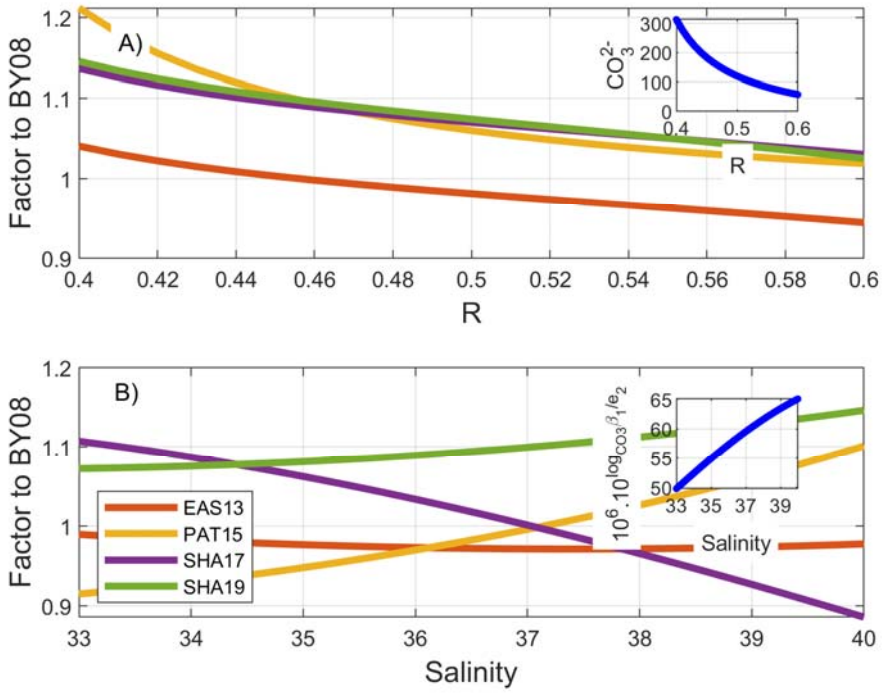

Figure S2. Comparison of the methodology approaches by EAS13, PAT15, SHA17, and SHA19 (Table S1) shown as factors with respect to the first approach by BY08: (A) $[CO_3^{2-}]_{spec}$ reported at 25 ºC and salinity 35 as a function of the Pb(II) absorbance ratio (R; Equation (2)), and (B) the term $\left[10^6 \cdot 10^{\log\left[\frac{CO_3\beta_1}{e_2}\right]}\right]$ in Equation (S4) as a function of salinity. The corresponding insets in each panel show absolute results with the BY08 approach (both in µmol·kg^{-1}; in blue).

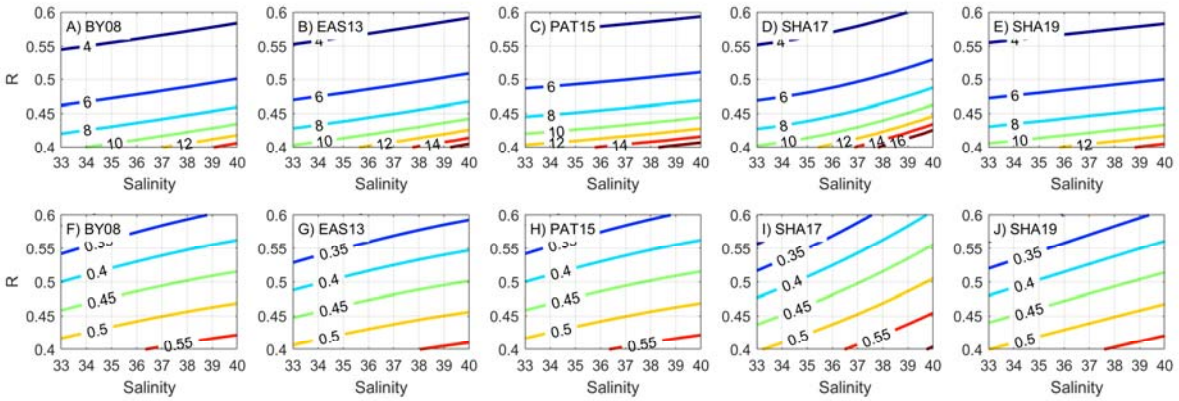

Figure S3. Comparison of the terms $[1/(R-e_1)]$ (upper row) and $[1-R\cdot e_3/e_2]$ (lower row) in Equation (S4) for the five approaches in Table S1 as a function of the absorbance ratio (R; Equation (2)) and salinity. The corresponding formulations are in Table S2. All axes are dimensionless.

Appendix C. Terminology

Terminology relative to measurement of CO_2 parameters

Accuracy. It refers to how close a measurement is to the correct (i.e., true) value for that measurement. Accuracy of CO_2 measurements is assessed against Certified Reference Materials (CRMs), if available. In the case of TA and DIC, there are CRMs[19] to assess the accuracy of the respective measurements. pH and $[CO_3^{2-}]_{spec}$ lack CRMs and their accuracy can only be examined against the respective calculated values, from the AT and DIC certified values of a CRM. In the case of pH, Tris buffer is also used as a standard material to compare against, although it is not considered a reference material.

Analytical Precision. It refers to how close is the agreement between repeated measurements that are repeated under the same conditions (i.e., the spread of the measured values one to another). In this study, precision is assessed as the standard deviation of a number of repeated measurements.

Total standard uncertainty. It is an estimate of how much your measured values deviate from a standard or expected value (i.e., the amount by which the measurement differs from the expected value). If measurements are not accurate or precise, then the uncertainty of the measurements will be very high. Sources of uncertainty can have either a random or a systematic origin. For $[CO_3^{2-}]_{spec}$, SHA19 described in detail the distinction between the random and systematic components of standard uncertainty;

- The random uncertainty refers to the analytical precision of the measurements. SHA19 estimated it at ± 0.7 % (Table S1).
- The systematic uncertainty refers to the uncertainty inherent to the fitting of the calibration functions (Table S2), which is based on $[CO_3^{2-}]_{calc}$ (Appendix B). This component of uncertainty can cause a bias in $[CO_3^{2-}]_{spec}$ due to the set of functions used. SHA19 estimated it at ±1.9 % in their approach.

The resulting combined (random plus systematic) total standard uncertainty assigned to $[CO_3^{2-}]_{spec}$ measurements amounts to ±2 % in SHA19, being consistent with previous approaches (Table S1). Hence, the total $[CO_3^{2-}]_{spec}$ standard uncertainty considers both the measurement imprecision and uncertainty inherent to the calibration functions.

Terminology relative to datasets description

In this study, dataset description applies to carbonate ion residuals shown in the results section.

Dispersion. Is a way of describing how scattered is a set of data. It refers to the variability or scatter of the data; when it is large, the data are widely scattered, while when it is small,

the data are clustered. Dispersion of data can be measured as the interquartile range (i.e. the difference between the 3rd and the 1st quartiles of the data; Figure 2) or as standard deviation (Table S4 and S5), among other measures of dispersion.

The dispersion of carbonate ion residuals is related to the random component of $[CO_3^{2-}]_{spec}$ uncertainty, through the photometric accuracy of the spectrophotometer used for measurement.

Bias. It refers to the observed trend in carbonate ion residuals with regard to $[CO_3^{2-}]_{calc}$. $[CO_3^{2-}]_{calc}$ residuals can be biased towards positive or negative values, within or beyond the ± 4 % limit for internal consistency.

The bias in carbonate ion residuals is related to the systematic component of $[CO_3^{2-}]_{spec}$ uncertainty, through the wavelength accuracy of the spectrophotometer used for measurement.

Terminology relative to measurement of absorbance

The spectrophotometer specifications (Table S3) impact the random and systematic components of $[CO_3^{2-}]_{spec}$ uncertainty, through the measurement of *R* (Equation (2)) values.

Table S3. Technical specifications of the spectrophotometer models used in the determination of $[CO_3^{2-}]_{spec}$ during the cruises shown in Table 1. Specifications of the spectrophotometer model (last column) used in the bibliography defining the $[CO_3^{2-}]_{spec}$ approaches (Table S1) are also shown. The estimated absorbance ratio random uncertainty (R random uncertainty), according to the photometric accuracy, is also shown. Photometric accuracy is in absorbance units (*A*).

	Shimadzu UV2401 (SHI2401)	**Shimadzu UV2600 (SHI2600)**	**Beckman DU800 (BK800)[a]**	**Perkin Elmer Lambda 850 (PE850)**	**Agilent UV8453**
Wavelength accuracy (nm)	± 0.3	± 0.3	± 0.5	± 0.08	± 0.5
Wavelength repeatability (nm)	± 0.1	± 0.05	± 0.2	± 0.02	± 0.02
Photometric Accuracy (*A*)	± 0.004	± 0.003	± 0.005	± 0.003	± 0.005
Stray Light (%)	< 0.015	< 0.005	< 0.05	< 0.00007	< 0.05
R random uncertainty	± 0.008	± 0.006	± 0.01	± 0.006	± 0.01

[a]All spectrophotometers are double beam except Beckman DU800 that is single beam. The Agilent UV8453 spectrophotometer, (Table S1) is also single beam.

Isosbestic point. In this study, it refers to the particular wavelength, in nanometers (nm), at which Pb(II) absorbance spectra shows the same value of absorbance at different conditions (i.e., at different $[CO_3^{2-}]$). This is, the value of absorbance does not depend on $[CO_3^{2-}]$.

Photometric accuracy. It marks the ability of the equipment to discern absorbance values within limits of confidence. It is a source of random uncertainty in *R*. A spectrophotometer with low photometric accuracy will introduce more random noise in *R* measurements, resulting in more dispersed *R* measurements. Table S3 shows the value of *R* random uncertainty for each spectrophotometer, according to their respective photometric accuracy.

Wavelength accuracy. It settles the capability of the equipment to read the absorbance at a given wavelength. It is a source of systematic uncertainty in *R*. This parameter can impact the accuracy of *R* measurements with regard to their true values and, thus, the goodness of the fitting of the set of functions (Table S2) due to the use of inaccurate *R* values. As reported in the Introduction and Appendix B, SAH17 proposed a correction to account for systematic offsets in *R* data (Equation (5)).

Wavelength repeatability. It is the stability of wavelength measurement. A measured wavelength should not drift within a range of wavelengths; it must be stable within a specified wavelength repeatability.

Stray light. This parameter introduces an error in the recorded absorbance, leading to negative deviations in Beer-Lambert's Law, causing increasing deviations as absorbance increases. It affects the signal-to-noise ratio, causing increasing photometric underestimation as absorbance increases. It is a source of random uncertainty in *R*.

Appendix D. $\Delta[CO_3^{2-}]$ uncertainty assessment: uncertainty in $[CO_3^{2-}]_{calc}$ estimation.

As described in Section 2.2 in the main text, the five sets of calibration functions (Table S2) reported for the determination of $[CO_3^{2-}]_{spec}$ in seawater were assessed through the study of the magnitude and distribution of carbonate ion residuals ($\Delta[CO_3^{2-}]$). In this regard, $[CO_3^{2-}]_{calc}$ are considered the reference or true values. The underlying reason for this is that the $[CO_3^{2-}]_{spec}$ methodology is itself defined according to $[CO_3^{2-}]_{calc,}$ through the characterization of the calibration functions that are fitted against $[CO_3^{2-}]_{calc}$, as explained in Appendix B.

The definition of $\Delta[CO_3^{2-}]$ ($[CO_3^{2-}]_{spec}$ - $[CO_3^{2-}]_{calc}$) in this study is the same as in EAS13, but opposite to BY08, PAT15, SHA17 and SHA19. $\Delta[CO_3^{2-}]$ are studied with regard $[CO_3^{2-}]_{calc}$, evaluating whether $[CO_3^{2-}]_{spec}$ are overestimated or underestimated regarding $[CO_3^{2-}]_{calc}$. Thus, $\Delta[CO_3^{2-}]$ indicate how close are $[CO_3^{2-}]_{spec}$ to the expected $[CO_3^{2-}]_{calc}$ values and, thus, how good is the performance of a set of calibration functions. Until a scientific agreement is achieved on what methodological approach is the best to measure the most accurate $[CO_3^{2-}]_{spec}$ and until a specific CRM will be available for this parameter, the five $[CO_3^{2-}]_{spec}$ obtained among approaches should be considered all potentially true values to be examined against $[CO_3^{2-}]_{calc}$ for accuracy.

With regard to $[CO_3^{2-}]_{calc}$ in this study, the following remarks should be considered:

1- Differences in $[CO_3^{2-}]_{calc}$ obtained from either the pH-TA and DIC-TA input pairs are small (blue dots in Figure S4), showing absolute values with a mean and standard deviation of 1.9 $\mu mol \cdot kg^{-1} \pm 1.5$ $\mu mol \cdot kg^{-1}$. As reported in the main text, all the results shown in this study were obtained with $[CO_3^{2-}]_{calc}$ from pH-TA.

2- The influence of the seawater model assumed for CO_2 system calculations, which relies on the different thermodynamic options for K_1 and K_2, K_{HSO4} and TB constants assumed for calculating $[CO_3^{2-}]_{calc}$, is small when the pH-TA input pair is considered, within 1 $\mu mol \cdot kg^{-1}$ (cyan dots in Figure S4). The two sets of thermodynamic constants tested with the CO2SYS package for MATLAB are (A) K_1K_2=10 (Lueker et al.[16]) and K_{HSO4} = 3 (Dickson[14] and Lee et al.[17]), and (B) K_1K_2 = 4 (Mehrbach et al.[12] as refit by Dickson and Millero[13]) and K_{HSO4} = 1 (Dickson[14] and Uppström[20]). Only these two sets of functions were used since these were the sets of constants used to assess $[CO_3^{2-}]_{calc}$ in the five evolving approaches of the methodology, as shown in Table S1.

3- If $[CO_3^{2-}]_{calc}$ total uncertainty is reevaluated by readjusting measured pH values to pH values that would have been obtained using purified dye, according to Liu et al.[21] (data for Sigma Aldrich, in their Figure 2), it increases by 0.8 % – 1.5 % over the $[CO_3^{2-}]_{calc}$ study range. Hence, the use of unpurified dye for pH measurements in the merged dataset in this study is not relevant for the interpretation and discussion of the reported results.

4 - The total uncertainty propagated in $[CO_3^{2-}]_{calc}$ through using the software *errors*, from Orr et al.,[22] is proportional to the concentration itself. It ranges between 2.5 µmol·kg^{-1} and 4.5 µmol·kg^{-1} for $[CO_3^{2-}]_{calc}$ obtained with the DIC-TA pair (black dots in Figure S4), and between 2.5 µmol·kg^{-1} and 8 µmol·kg^{-1} for the pH-TA pair (red dots in Figure S4) within the $[CO_3^{2-}]_{calc}$ study range (68 µmol·kg^{-1} – 252 µmol·kg^{-1}), so from 3.7 % to 1.8 % with DIC-TA and from 3.7 % to 3.2 % with pH-TA.

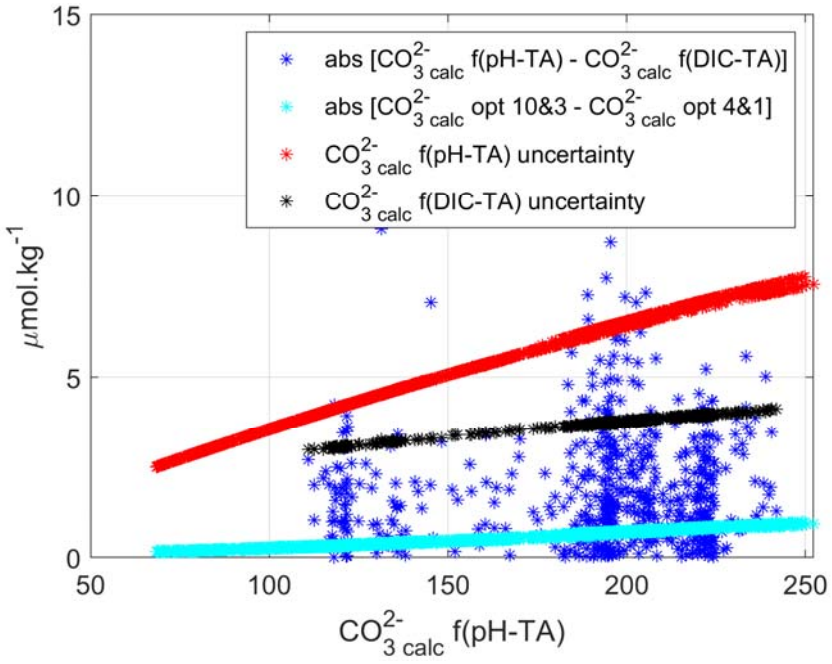

Figure S4. Sources of uncertainty in the calculated carbonate ion content ($[CO_3^{2-}]_{calc}$, in µmol·kg^{-1}) based on the dataset of this study. All data are shown as absolute values. Blue symbols show the difference in $[CO_3^{2-}]_{calc}$ between data estimated with the pH-TA and DIC-TA input pairs. The cyan symbols depict the range of differences between $[CO_3^{2-}]_{calc}$ obtained from the pH-TA pair using two thermodynamic options in the CO2SYS package for MATLAB[23] [K_1K_2 = 10 (Lueker et al.[16]) and K_{HSO4} = 3 (Dickson[14] & Lee et al.[17]) and K_1K_2 = 4 (Mehrbach et al.,[12] as refit by Dickson and Millero[13]) and K_{HSO4} = 1 (Dickson[14] and Uppström[20])]. The black and red symbols depict the combined standard uncertainty in $[CO_3^{2-}]_{calc}$ estimated from DIC-TA and pH-TA input pairs, respectively, based on the *errors* script by Orr et al.[22] [standard uncertainties: 0.01 for pH, ± 3 µmol·kg^{-1} for DIC or TA (Section 2.1) and those in Table 1 in Orr et al.[22] for the constants].

Mean $\Delta[CO_3^{2-}]$ and standard deviation for each cruise in this study are shown in Table S4 (for the whole range of amount of $[CO_3^{2-}]_{calc}$ content) and Table S5 (for low, medium, and high ranges of amount of $[CO_3^{2-}]_{calc}$ content). Note that Tables S4 and S5 and the respective captions are shown in separated pages due to space reasons.

Table S4. Mean ± standard deviation values of $\Delta[CO_3^{2-}]$ ($\Delta[CO_3^{2-}] = [CO_3^{2-}]_{spec} - [CO_3^{2-}]_{calc}$; in $\mu mol \cdot kg^{-1}$) for each of the cruises in Table 1. The number of samples averaged is shown in parenthesis. The cruise alias and the spectrophotometer (SHI2401, SHI2600, PE850, or BK800; Table S3) used are indicated in the column headers. $[CO_3^{2-}]_{spec}$ is calculated with five different formulations: BY08, EAS13, PAT15, SHA17, and SHA19 (Table S2); and $\Delta[CO_3^{2-}]$ from data measured with $PbCl_2$ or $Pb(ClO_4)_2$ are shown separately. $[CO_3^{2-}]_{calc}$ is calculated with pH and TA. Calculations are at 25 ºC and 1 atm except for SHA19 that is at 1 atm and the exact temperature of analysis. The SHA17 and SHA19 approaches include a wavelength correction ($\Delta\lambda$; Table S1) that equals 0.2 nm for cruises where the SHI2600 was used (HOTMIX, MSM72, RADPROF, RADCOR, and iFADO; Table 1) and is null for the remaining cases. $\Delta[CO_3^{2-}] < 4$ %, 4 % < $\Delta[CO_3^{2-}] < 10$ %, or $\Delta[CO_3^{2-}] > 10$ % are highlighted in green, orange and red, respectively.

Table S5. Mean ± standard deviation values of $\Delta[CO_3^{2-}]$ ($\Delta[CO_3^{2-}] = [CO_3^{2-}]_{spec} - [CO_3^{2-}]_{calc}$; in $\mu mol \cdot kg^{-1}$) for each of the cruises in Table 1 for three different $[CO_3^{2-}]_{calc}$ ranges: $[CO_3^{2-}]_{calc} < 100$ $\mu mol \cdot kg^{-1}$, $100 < [CO_3^{2-}]_{calc} < 180$ $\mu mol \cdot kg^{-1}$, and $[CO_3^{2-}]_{calc} > 180$ $\mu mol \cdot kg^{-1}$, shown in the upper, middle and lower lines within each cell, respectively. The number of samples is shown in parenthesis. The cruise alias and the spectrophotometer (SHI2401, SHI2600, PE850, or BK800; Table S3) used are indicated in the column headers. $[CO_3^{2-}]_{spec}$ is calculated with five different formulations: BY08, EAS13, PAT15, SHA17, and SHA19 (Table S2); and $\Delta[CO_3^{2-}]$ from data measured with $PbCl_2$ or $Pb(ClO_4)_2$ are shown separately. $[CO_3^{2-}]_{calc}$ is calculated with pH and TA. Calculations are reported at 25 ºC and 1 atm except for SHA19 that is reported at 1 atm and the exact temperature of analysis. The SHA17 and SHA19 approaches include a wavelength correction ($\Delta\lambda$; Table S1) that equals 0.2 nm for cruises where the SHI2600 was used (HOTMIX, MSM72, RADPROF, RADCOR, and iFADO; Table 1) and is null for the remaining cases. $\Delta[CO_3^{2-}] < 4$ %, 4 % < $\Delta[CO_3^{2-}] < 10$ %, or $\Delta[CO_3^{2-}] > 10$ % are highlighted, in green, orange and red, respectively.

Table S4

		CAIBOX PE850	MOC2 SHI2401	HOTMIX SHI2600	OVIDE PE850	TALPRO BK800	MEDWAVES PE850	MSM72 SHI2600	RADPROF SHI2600	RADCOR SHI2600	iFADO SHI2600	iFADO 2 PE850
BY08	$PbCl_2$	4.2 ± 2.7 (272)	1 ± 4 (625)	-4.7 ± 5.6 (321)	0.6 ± 2.8 (196)				4.4 ± 3.7 (48)	0.8 ± 6.2 (127)	1.9 ± 1.5 (28)	-4.5± 3.1 (33)
	$Pb(ClO_4)_2$					-5.4 ± 11.6 (111)	-12.8 ± 3.6 (294)	-12.8 ± 3.6 (294)	-1.0 ± 2.7 (44)	1.4 ± 5.7 (72)	-4.6 ± 3.3 (32)	-11.2 ± 3.3 (34)
EAS13	$PbCl_2$	2.5 ± 2.7 (272)	-0.8 ± 3.5 (625)	-5.4 ± 5.4 (321)	-1.4 ± 2.9 (196)				2.6 ± 4.1 (48)	0.3 ± 6.2 (127)	-0.1 ± 1.8 (28)	-6.4 ± 3.1 (33)
	$Pb(ClO_4)_2$					-6.3 ± 12.1 (111)	-21.3 ± 6.2 (147)	-13.8 ± 3.5 (294)	-3.1 ± 2.9 (44)	0.2 ± 5.6 (72)	-6.8 ± 3 (32)	-13.3 ± 2.8 (34)
PAT15	$PbCl_2$	24.4 ± 7.7 (272)	17.4 ± 10.4 (625)	33.9 ± 7.9 (321)	17.2 ± 4.9 (196)				22.9 ± 6.3 (48)	26.2 ± 7.7 (127)	20 ± 5.6 (28)	14.2 ± 5.4 (33)
	$Pb(ClO_4)_2$					35.0 ± 14.4 (111)	-0.4 ± 3.2 (147)	27.7 ± 4.7 (294)	16.2 ± 4.9 (44)	25.0 ± 5.9 (72)	12.2 ± 3.2 (32)	5.8 ± 2.4 (34)
SHA17	$PbCl_2$	16.2 ± 5.1 (272)	10.6 ± 6.2 (625)	9.4 ± 4.4 (321)	10.4 ± 3.5 (196)				8.8 ± 4.1 (48)	7.2 ± 6.5 (127)	6.1 ± 2.4 (28)	6.5 ± 3.8 (33)
	$Pb(ClO_4)_2$					20.6 ± 13.9 (111)	-8.1 ± 3.6 (147)	2.5 ± 3.6 (294)	2.9 ± 2.9 (44)	7.3 ± 5.6 (72)	-0.8 ± 2.6 (32)	-1.2 ± 1.4 (34)
SHA19	$PbCl_2$	20.3 ± 5.7 (272)	12.6 ± 6.7 (625)	12.6 ± 6.7 (625)	11.4 ± 3.8 (196)				10.8 ± 4.2 (48)	9.8 ± 5.9 (127)	7.3 ± 2.5 (28)	6.0 ± 3.8 (33)
	$Pb(ClO_4)_2$					22.6 ± 13.5 (111)	-7.4 ± 3.4 (147)	0.7 ± 3.1 (294)	4.8 ± 3.1 (44)	8.6 ± 4.6 (72)	0.1 ± 2.4 (32)	-1.7 ± 1.7 (34)

Table S5		CAIBOX PE850	MOC2 SHI2401	HOTMIX SHI2600	OVIDE PE850	TALPRO BK800	MEDWAVES PE850	MSM72 SHI2600	RADPROF SHI2600	RADCOR SHI2600	iFADO SHI2600	iFADO 2 PE850
BY08	$PbCl_2$	---------- 4.5 ± 2.4 (236) 2.7 ± 4.1 (36)	2.3 ± 1.7 (238) 1.6 ± 3.2 (299) -4.3 ± 6.3 (88)	---------- 1.8 ± 2.5 (47) -5.8 ± 5.3 (274)	---------- 0.7 ± 2.7 (188) -2.4 ± 3.3 (8)				---------- 4.3 ± 3.8 (45) 6.1 ± 3.1 (3)	---------- 1.4 ± 5.3 (98) -1.1 ± 8.1 (29)	---------- 1.8 ± 1.5 (25) 2.6 ± 1.6 (3)	---------- -4 ± 2.5 (26) -6.3 ± 4.5 (7)
	$Pb(ClO_4)_2$					---------- ---------- 5.4 ± 11.6 (111)	---------- -16 ± 4.0 (114) -28.4 ± 3.4 (33)	---------- -9.9 ± 2.7 (3) -12.9 ± 3.6 (291)	---------- -1 ± 2.7 (41) -1.9 ± 1.7 (3)	---------- 2.3 ± 5.2 (62) -4.6 ± 4.6 (10)	---------- -3.6 ± 1.6 (28) -11.7 ± 3.7 (4)	---------- 9.8 ± 1.8 (27) -16.4 ± 2.3 (7)
EAS13	$PbCl_2$	---------- 2.4 ± 2.4 (236) 3.2 ± 4.2 (36)	-0.5 ± 1.7 (238) -0.7 ± 3.3 (299) -1.9 ± 6.5 (88)	---------- -0.4 ± 2.6 (47) -6.2 ± 5.2 (274)	---------- -1.4 ± 2.9 (188) -2.2 ± 3.6 (8)				---------- 2.3 ± 4 (45) 6.6 ± 3.3 (3)	---------- 0.6 ± 5.5 (98) -0.6 ± 8.3 (29)	---------- -0.4 ± 1.5 (25) 2.6 ± 1.6 (3)	---------- -6.3 ± 2.5 (26) -6.7 ± 4.9 (7)
	$Pb(ClO_4)_2$					---------- ---------- 6.3 ± 12.1 (111)	---------- -18.7 ± 3.9 (114) -30.3 ± 3.5 (33)	---------- -11.9 ± 3.2 (3) -13.8 ± 3.5 (291)	---------- -3.2 ± 2.9 (41) -1.9 ± 1.7 (3)	---------- 1.0 ± 5.3 (62) -4.6 ± 4.8 (10)	---------- -6 ± 1.8 (28) -12.4 ± 3.9 (4)	---------- -12.3 ± 1.9 (27) -17.3 ± 2.3 (7)
PAT15	$PbCl_2$	---------- 22 ± 4.3 (236) 40.0 ± 6.2 (36)	10.7 ± 2.2 (238) 16.3 ± 4.5 (299) 39.5 ± 8.2 (88)	---------- 19.7 ± 4.6 (47) 36.3 ± 5.4 (274)	---------- 16.7 ± 4.2 (188) 29.0 ± 4.5 (8)				---------- 21.9 ± 5.0 (45) 38.1 ± 4.1 (3)	---------- 25.5 ± 6.7 (98) 28.8 ± 10.1 (29)	---------- 18.4 ± 3.1 (25) 33.3 ± 1.5 (3)	---------- 12.1 ± 2.7 (26) 21.9 ± 6.2 (7)
	$Pb(ClO_4)_2$					---------- ---------- 35.0 ± 14.4 (111)	---------- -0.7 ± 2.6 (114) 0.4 ± 4.8 (33)	---------- 20.4 ± 0.6 (3) 27.8 ± 4.7 (291)	---------- 15.3 ± 3.8 (41) 27.9 ± 2.2 (3)	---------- 25.2 ± 5.9 (62) 23.8 ± 5.9 (10)	---------- 11.8 ± 2.9 (28) 14.9 ± 4.5 (4)	---------- 5.0 ± 1.3 (27) 9.2 ± 2.7 (7)
SHA17	$PbCl_2$	---------- 14.8 ± 3.2 (236) 25.4 ± 5.3 (36)	6.9 ± 2 (238) 10.2 ± 3.7 (299) 22 ± 7.2 (88)	---------- 6 ± 2.7 (47) 10.0 ± 4.4 (274)	---------- 10.1 ± 3.3 (188) 16.3 ± 4 (8)				---------- 8.4 ± 3.9 (45) 14.4 ± 3.3 (3)	---------- 7.4 ± 5.7 (98) 6.5 ± 8.7 (29)	---------- 5.6 ± 1.8 (25) 10.6 ± 1.6 (3)	---------- 5.4 ± 2.3 (26) 10.5 ± 5.5 (7)
	$Pb(ClO_4)_2$					---------- ---------- 20.6 ± 13.9 (111)	---------- -7.2 ± 2.8 (114) -11.4 ± 4.2 (33)	---------- -0.4 ± 1.1 (3) 2.5 ± 3.6 (291)	---------- 2.7 ± 2.8 (41) 5.8 ± 1.7 (3)	---------- 8 ± 5.4 (62) 2.6 ± 5 (10)	---------- -0.2 ± 1.8 (28) -4.9 ± 3.9 (4)	---------- -1.2 ± 1.0 (27) -1.2 ± 2.5 (7)
SHA19	$PbCl_2$	---------- 18.6 ± 3.5 (236) 31.5 ± 4.1 (36)	8.1 ± 2 (238) 12.3 ± 3.9 (299) 25.5 ± 6.4 (88)	---------- 6.0 ± 2.9 (47) 8.6 ± 4.3 (274)	---------- 11.1 ± 3.4 (188) 18.3 ± 5 (8)				---------- 10.3 ± 3.8 (45) 18.0 ± 3.4 (3)	---------- 9.1 ± 5.4 (98) 12.3 ± 7 (29)	---------- 6.7 ± 1.7 (25) 12.7 ± 2.1 (3)	---------- 4.9 ± 2.8 (26) 9.9 ± 4.8 (7)
	$Pb(ClO_4)_2$					---------- ---------- 22.6 ± 13.5 (111)	---------- -6.5 ± 2.7 (114) -10.3 ± 4.0 (33)	---------- 0.6 ± 1.9 (3) 0.7 ± 3.1 (291)	---------- 4.5 ± 2.9 (41) 9.3 ± 1.7 (3)	---------- 9.1 ± 4.5 (62) 5.3 ± 3.8 (10)	---------- 0.6 ± 1.9 (28) -3.4 ± 2.9 (4)	---------- -1.6 ± 1.3 (27) -1.8 ± 2.9 (7)

Appendix E. $\Delta[CO_3^{2-}]$ uncertainty assessment: $[CO_3^{2-}]_{spec}$ uncertainty related to the absorbance ratio. Monte Carlo analysis.

The random uncertainty inherent to the methodology for $[CO_3^{2}]_{spec}$ determination was tested with a Monte Carlo analysis. To examine the minimum random errors that could be ascribed to *R* measurements, the value of ±0.006 was selected to perform the corresponding perturbations, because it is the lowest value for *R* uncertainty derived from the respective photometric accuracy specifications of all spectrophotometers used in this study (Table S3). It derives from PE850 and SHI2600, in particular.

The Monte Carlo analysis modifies *R* measurements according to a random value from a normal distribution with a mean of zero and a standard deviation of 0.006/2. The perturbed *R* values are used with the EAS13 approach to obtain $[CO_3^{2}]_{spec}$ perturbed values that are used to calculate $\Delta[CO_3^{2-}]$. Figure S5 shows the corresponding results for *R* data measured with $PbCl_2$, highlighting that $\Delta[CO_3^{2-}]$ have larger random uncertainty at higher values of $[CO_3^{2-}]_{calc}$, particularly at $[CO_3^{2-}]_{calc} > 180$ µmol·kg^{-1}. The same results were found for data measured with $Pb(ClO_4)_2$ (data not shown). Consequently, even higher random uncertainty would be expected for *R* data measured with the remaining spectrophotometers (BK800 and SHI2401), including the model used for defining the spectrophotometric parameters in Equation (S4), UV8453, since all of them have higher uncertainty in photometric accuracy than PE850 and SHI2600 (Table S3).

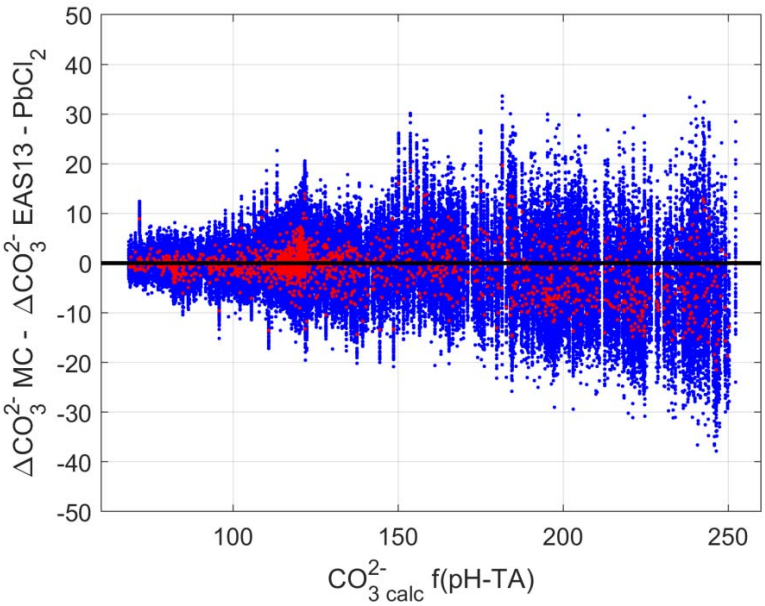

Figure S5. Red dots correspond to $[CO_3^{2-}]_{spec}$ obtained with the EAS13 approach minus $[CO_3^{2-}]_{calc}$ ($\Delta[CO_3^{2-}]$-EAS13 = $[CO_3^{2-}]_{spec}$ - $[CO_3^{2-}]_{calc}$; in µmol·kg^{-1}) as a function of $[CO_3^{2-}]_{calc}$ (calculated from pH and TA), for all $PbCl_2$ data among cruises in Table 1. Blue dots correspond to a Monte Carlo analysis showing the difference between $\Delta[CO_3^{2-}]$-MC and $\Delta[CO_3^{2-}]$-EAS13. $\Delta[CO_3^{2-}]$-MC correspond to perturbed $[CO_3^{2-}]_{spec}$ determined with the EAS13 approach (but on *R* data perturbed introducing random errors of ±0.006) minus $[CO_3^{2-}]_{calc}$ (in µmol·kg^{-1}).

Appendix F: $\Delta[CO_3^{2-}]$ uncertainty assessment: $[CO_3^{2-}]_{spec}$ uncertainty related to the absorbance ratio. Absorbance measurements with both Pb(II) reagents and different spectrophotometers.

During the RADPROF and iFADO cruises, discrete *R* values were measured on replicate samples, using $PbCl_2$ and $Pb(ClO_4)_2$ to obtain $[CO_3^{2-}]_{spec}$ with the SHI2600 (Table 1). During the iFADO cruise, both SHI2600 and PE850 were used with the two reagents for measuring discrete *R* values. Additionally, during the iFADO cruise, scan readings from 220 nm to 370 nm were performed in quadruplicate samples. Using both reagents and SHI2600 and PE850, three to five scans per sample were recorded with sampling intervals of 0.5 nm or 1 nm, in different exercises, and averaged to obtain a mean and standard deviation absorbance value by wavelength. Mean and standard deviation absorbances were obtained at discrete target wavelengths, λ, from each mean scan by averaging values about ± 2 nm from the target λ: ${}_{234}A$, ${}_{250}A$ and ${}_{350}A$. Corresponding results by reagent and spectrophotometer are shown in Figures S6 and S7.

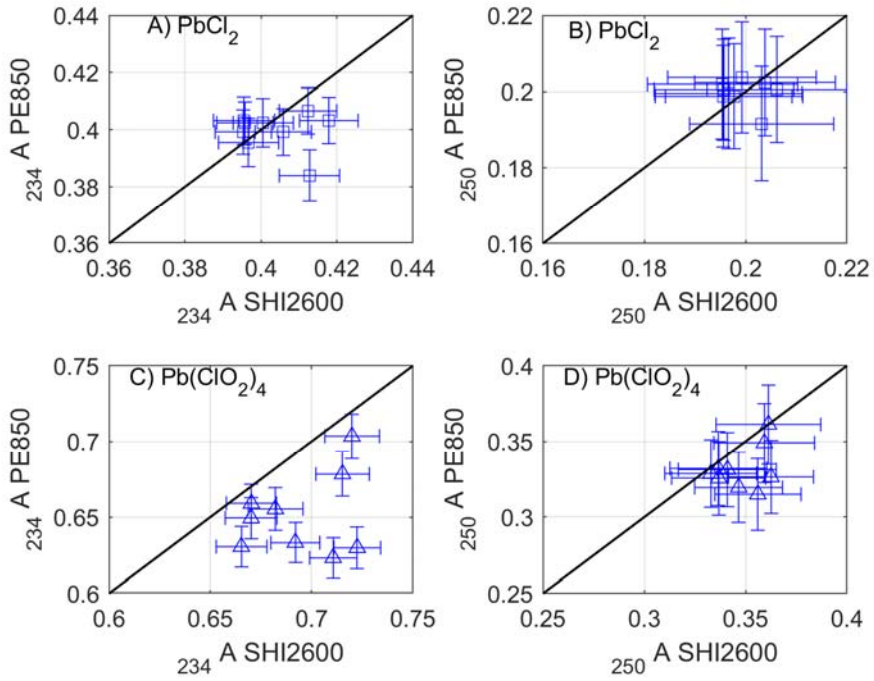

Figure S6. Comparison of Pb(II) absorbance between the SHI2600 and the PE850 spectrophotometers at (A, C) λ= 234 nm and (B, D) λ= 250 nm wavelengths for sample replicates measured using $PbCl_2$ (upper panels) and $Pb(ClO_4)_2$ (lower panels) during the iFADO cruise. Absorbance readings at 234 nm and 250 nm are corrected for the background absorbance at 350 nm. Points and error bars correspond to the mean and standard deviations of absorbance measurements about ± 2 nm from the target λ values.

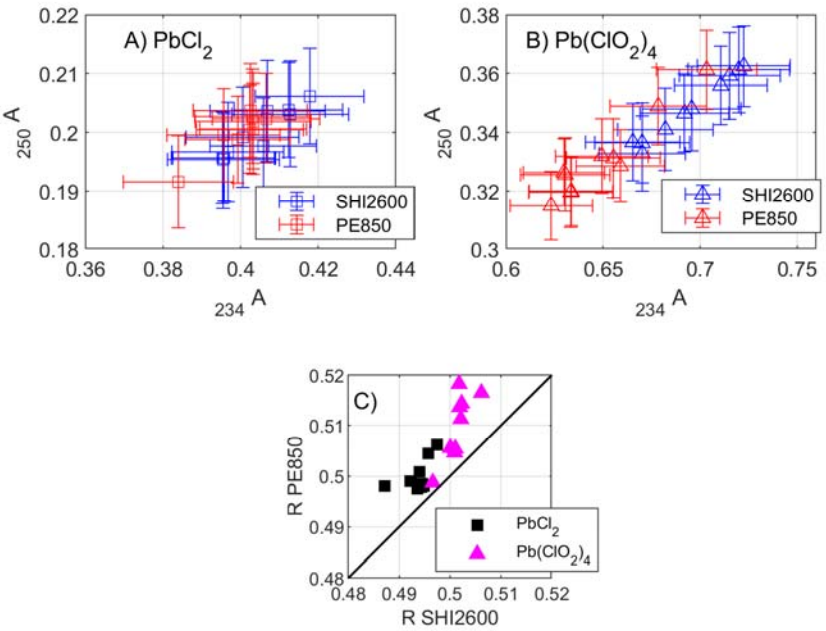

Figure S7. Relationship between Pb(II) absorbance at λ = 234 nm and λ = 250 nm wavelengths for sample replicates measured with the SHI2600 (in blue) and the PE850 (in red) spectrophotometers, using (A) $PbCl_2$ and (B) $Pb(ClO_4)_2$ during the iFADO cruise. Both absorbance readings are corrected for the background absorbance at 350 nm. Points and error bars correspond to the mean and standard deviations of absorbance measurements about ± 2 nm from the target λ values. (C) Comparison of *R* values ($R = [({}_{250}A - {}_{350}A)/({}_{234}A - {}_{350}A)]$) between spectrophotometers using $PbCl_2$ (black squares) and $Pb(ClO_4)_2$ (pink triangles).

REFERENCES

(1) Chung, S.-N.; Park, G.-H.; Lee, K.; Key, R. M.; Millero, F. J.; Feely, R. A.; Sabine, C. L.; Falkowski, P. G. Postindustrial Enhancement of Aragonite Undersaturation in the Upper Tropical and Subtropical Atlantic Ocean: The Role of Fossil Fuel CO_2. *Limnology and Oceanography* **2004**, *49* (2), 315–321. https://doi.org/10.4319/lo.2004.49.2.0315.

(2) Jiang, L.-Q.; Feely, R. A.; Carter, B. R.; Greeley, D. J.; Gledhill, D. K.; Arzayus, K. M. Climatological Distribution of Aragonite Saturation State in the Global Oceans. *Global Biogeochemical Cycles* **2015**, *29* (10), 1656–1673. https://doi.org/10.1002/2015GB005198.

(3) Zeebe, R. E.; Wolf-Gladrow, D. *CO_2 in Seawater: Equilibrium, Kinetics, Isotopes*; Elsevier Science, 2001; Vol. 65.

(4) Egleston, E. S.; Sabine, C. L.; Morel, F. M. M. Revelle Revisited: Buffer Factors That Quantify the Response of Ocean Chemistry to Changes in DIC and Alkalinity. *Global Biogeochemical Cycles* **2010**, *24* (1). https://doi.org/10.1029/2008GB003407.

(5) Olsen, A.; Lange, N.; Key, R. M.; Tanhua, T.; Álvarez, M.; Becker, S.; Bittig, H. C.; Carter, B. R.; Cotrim da Cunha, L.; Feely, R. A.; van Heuven, S.; Hoppema, M.; Ishii, M.; Jeansson, E.; Jones, S. D.; Jutterström, S.; Karlsen, M. K.; Kozyr, A.; Lauvset, S. K.; Lo Monaco, C.; Murata, A.; Pérez, F. F.; Pfeil, B.; Schirnick, C.; Steinfeldt, R.; Suzuki, T.; Telszewski, M.; Tilbrook, B.; Velo, A.; Wanninkhof, R. GLODAPv2.2019 – an Update of GLODAPv2. *Earth Syst. Sci. Data* **2019**, *11* (3), 1437–1461. https://doi.org/10.5194/essd-11-1437-2019.

(6) Byrne, R. H.; Yao, W. Procedures for Measurement of Carbonate Ion Concentrations in Seawater by Direct Spectrophotometric Observations of Pb(II) Complexation. *Marine Chemistry* **2008**, *112* (1), 128–135. https://doi.org/10.1016/j.marchem.2008.07.009.

(7) Easley, R. A.; Patsavas, M. C.; Byrne, R. H.; Liu, X.; Feely, R. A.; Mathis, J. T. Spectrophotometric Measurement of Calcium Carbonate Saturation States in Seawater. *Environ. Sci. Technol.* **2013**, *47* (3), 1468–1477. https://doi.org/10.1021/es303631g.

(8) Patsavas, M. C.; Byrne, R. H.; Yang, B.; Easley, R. A.; Wanninkhof, R.; Liu, X. Procedures for Direct Spectrophotometric Determination of Carbonate Ion Concentrations: Measurements in US Gulf of Mexico and East Coast Waters. *Marine Chemistry* **2015**, *168*, 80–85. https://doi.org/10.1016/j.marchem.2014.10.015.

(9) Sharp, J. D.; Byrne, R. H.; Liu, X.; Feely, R. A.; Cuyler, E. E.; Wanninkhof, R.; Alin, S. R. Spectrophotometric Determination of Carbonate Ion Concentrations: Elimination of Instrument-Dependent Offsets and Calculation of In Situ Saturation States. *Environ. Sci. Technol.* **2017**, *51* (16), 9127–9136. https://doi.org/10.1021/acs.est.7b02266.

(10) Sharp, J. D.; Byrne, R. H. Carbonate Ion Concentrations in Seawater: Spectrophotometric Determination at Ambient Temperatures and Evaluation of Propagated Calculation Uncertainties. *Marine Chemistry* **2019**, *209*, 70–80. https://doi.org/10.1016/j.marchem.2018.12.001.

(11) Easley, R. A.; Byrne, R. H. The Ionic Strength Dependence of Lead (II) Carbonate Complexation in Perchlorate Media. *Geochimica et Cosmochimica Acta* **2011**, *75* (19), 5638–5647. https://doi.org/10.1016/j.gca.2011.07.007.

(12) Mehrbach, C.; Culberson, C. H.; Hawley, J. E.; Pytkowicx, R. M. Measurement of the Apparent Dissociation Constants of Carbonic Acid in Seawater at Atmospheric Pressure. *Limnology and Oceanography* **1973**, *18* (6), 897–907. https://doi.org/10.4319/lo.1973.18.6.0897.

(13) Dickson, A. G.; Millero, F. J. A Comparison of the Equilibrium Constants for the Dissociation of Carbonic Acid in Seawater Media. *Deep Sea Research Part A. Oceanographic Research Papers* **1987**, *34* (10), 1733–1743. https://doi.org/10.1016/0198-0149(87)90021-5.

(14) Dickson, A. G. Standard Potential of the Reaction: AgCl(s) + $12H_2$(g) = Ag(s) + HCl(Aq), and and the Standard Acidity Constant of the Ion HSO_4^- in Synthetic Sea Water from 273.15 to 318.15 K. *The Journal of Chemical Thermodynamics* **1990**, *22* (2), 113–127. https://doi.org/10.1016/0021-9614(90)90074-Z.

(15) Dickson, A. G. Thermodynamics of the Dissociation of Boric Acid in Synthetic Seawater from 273.15 to 318.15 K. *Deep Sea Research Part A. Oceanographic Research Papers* **1990**, *37* (5), 755–766. https://doi.org/10.1016/0198-0149(90)90004-F.

(16) Lueker, T. J.; Dickson, A. G.; Keeling, C. D. Ocean $_pCO_2$ Calculated from Dissolved Inorganic Carbon, Alkalinity, and Equations for K_1 and K_2: Validation Based on Laboratory Measurements of CO_2 in Gas and Seawater at Equilibrium. *Marine Chemistry* **2000**, *70* (1), 105–119. https://doi.org/10.1016/S0304-4203(00)00022-0.

(17) Lee, K.; Kim, T.-W.; Byrne, R. H.; Millero, F. J.; Feely, R. A.; Liu, Y.-M. The Universal Ratio of Boron to Chlorinity for the North Pacific and North Atlantic Oceans. *Geochimica et Cosmochimica Acta* **2010**, *74* (6), 1801–1811. https://doi.org/10.1016/j.gca.2009.12.027.

(18) Fajar, N. M.; García-Ibáñez, M. I.; SanLeón-Bartolomé, H.; Álvarez, M.; Pérez, F. F. Spectrophotometric Measurements of the Carbonate Ion Concentration: Aragonite Saturation States in the Mediterranean Sea and Atlantic Ocean. *Environ. Sci. Technol.* **2015**, *49* (19), 11679–11687. https://doi.org/10.1021/acs.est.5b03033.

(19) Dickson, A. G.; Afghan, J. D.; Anderson, G. C. Reference Materials for Oceanic CO_2 Analysis: A Method for the Certification of Total Alkalinity. *Marine Chemistry* **2003**, *80* (2), 185–197. https://doi.org/10.1016/S0304-4203(02)00133-0.

(20) Uppström, L. R. The Boron/Chlorinity Ratio of Deep-Sea Water from the Pacific Ocean. *Deep Sea Research and Oceanographic Abstracts* **1974**, *21* (2), 161–162. https://doi.org/10.1016/0011-7471(74)90074-6.

(21) Liu, X.; Patsavas, M. C.; Byrne, R. H. Purification and Characterization of Meta-Cresol Purple for Spectrophotometric Seawater PH Measurements. *Environ. Sci. Technol.* **2011**, *45* (11), 4862–4868. https://doi.org/10.1021/es200665d.

(22) Orr, J. C.; Epitalon, J.-M.; Dickson, A. G.; Gattuso, J.-P. Routine Uncertainty Propagation for the Marine Carbon Dioxide System. *Marine Chemistry* **2018**, *207*, 84–107. https://doi.org/10.1016/j.marchem.2018.10.006.

(23) Van Heuven, S.; Pierrot, D.; Rae, J. W. B.; Lewis, E.; Wallace, D. W. R. MATLAB Program Developed for CO_2 System Calculations. *ORNL/CDIAC-105b* **2011**, *530*.